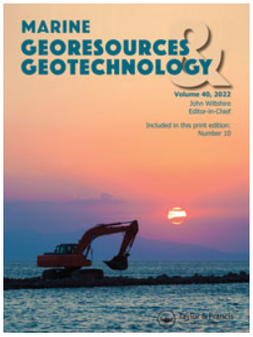

Marine Georesources & Geotechnology

ISSN: (Print) (Online) Journal homepage: https://www.tandfonline.com/loi/umgt20

Shale-gas potential from Cretaceous succession in South Africa's Orange Basin: Insights from integrated geochemical evaluations

Nura Abdulmumini Yelwa, Khairul Azlan Mustapha, Mimonitu Opuwari & Mohammed Hail Hakimi

To cite this article: Nura Abdulmumini Yelwa, Khairul Azlan Mustapha, Mimonitu Opuwari & Mohammed Hail Hakimi (2022): Shale-gas potential from Cretaceous succession in South Africa's Orange Basin: Insights from integrated geochemical evaluations, Marine Georesources & Geotechnology, DOI: 10.1080/1064119X.2022.2118647

To link to this article: https://doi.org/10.1080/1064119X.2022.2118647

MARINE GEORESOURCES & GEOTECHNOLOGY
https://doi.org/10.1080/1064119X.2022.2118647

Shale-gas potential from Cretaceous succession in South Africa's Orange Basin: Insights from integrated geochemical evaluations

Nura Abdulmumini Yelwa[a,b], Khairul Azlan Mustapha[a], Mimonitu Opuwari[c] and Mohammed Hail Hakimi[d]

[a]Department of Geology, University of Malaya, Kuala Lumpur, Malaysia; [b]Department of Geology, Faculty of Physical and Computing Sciences, Usmanu Danfodiyo University Sokoto, Sokoto, Nigeria; [c]Earth Sciences Department, University of the Western Cape, Cape Town, South Africa; [d]Geology Department, Faculty of Applied Science, Taiz University, Taiz, Yemen

ABSTRACT

Shale sediments were collected from four Cretaceous stratigraphic units across four explorations well locations in South Africa's Orange Basin and analysed to determine organic-matter characteristics, such as amount, quality, thermal maturity, and their viability as gas resources. The geochemical results show that the Cretaceous shales contain moderate organic quantities, as shown by TOC averagely up to 1.29%. The organic facies consist primarily of Type III kerogen, as proven alongside low hydrogen indexes between 40 and 133 mg HC/g TOC. As seen under a reflected light microscope, the dominance of such land plant-rich organic matter is in harmony with the significant amount of Vitrinite macerals. These organic sediments can produce primarily gas when they mature. The geological and geochemical properties of the organic sediments, chiefly Type III kerogen, generate both wet and dry gas, particularly when adequate thermal maturity is enhanced at deeper locations. Thus, the Orange Basin is considered promising for shale gas exploration and production.

ARTICLE HISTORY
Received 1 March 2022
Accepted 28 July 2022

KEYWORDS
Shale gas; source rocks; Orange Basin; organic matter; kerogen

1. Introduction

The Orange Basin has established a seaward Southwest African Atlantic boundary of approximately 160,000 km^2, extending from the shelf to the deep offshore marine (Figure 1). Although it is South Africa's most extensive offshore basin, it is fairly understudied, with only 40 boreholes, one well for every 4000 km^2 (Broad et al. 2012). Earlier work in the region was not confined to geochemical, geophysical, and sedimentological analyses. Some noble geochemical research was undertaken (Van der Spuy 2003; Hirsch et al. 2010; Adekola and Akinlua 2012; Alexander Hartwig, Anka, and di Primio 2012; Adekola, Akinlua, and Mangelsdorf 2012; Akinlua et al. 2015; Yelwa et al. 2022), though few studies highlighted the geochemical properties of Orange Basin shales.

A petroleum system includes various key elements, including the source rock, the migration path, the reservoir rock, the seal and the overload (Magoon and Dow 1994). The processes of this system involve generating, expelling, accumulating, overburdening and hydrocarbon preservation (Magoon and Dow 1994). Absorption of petroleum is also a necessary process to understand shales' gases in place (GIP) (Jarvie et al. 2007). However, this may cause a specific residual oil discharge or possible mechanical cracking (Sandvik, Young, and Curry 1992; Stainforth and Reinders 1990; Thomas and Clouse 1990).

The recent breakthrough of unconventional hydrocarbon systems, particularly those which recognize source-rock reservoirs, i.e., organic-rich mudstone that serves as both a source and a reservoir rock, has resulted in a re-evaluation of fundamental and critical geological processes operating in fine-grained sediments (Jarvie et al. 2007; Schmoker et al. 1995; Sohail, Radwan, and Mahmoud 2022; Taylor and Macquaker 2014). A non-conventional, continuous petroleum system is made up of hydrocarbons located in low-matrix-permeability rocks that rely on fracture pore size distribution (naturally or artificially) for yield and contain high levels of petroleum, although with reduced gas recovery constraints (Jarvie et al. 2007; Schmoker et al. 1995). As a result, the behaviour of shale gas somewhere within a nanoscale area is becoming a cause of worry for scientists that want to evaluate the tap prospects of a specific shale gas reservoir and use this to enhance biogas yield.

Since the first large-scale shale gas breakthrough in the United States in 1821 from Devonian organic-rich shale, shale petroleum has received much interest in North America as an essential source of energy (Curtis 2002; Jarvie et al. 2007). America appeared to be the first and most prosperous country in developing and utilizing shale gas effectively (Xingang, Jiaoli, and Bei 2013; Li et al. 2018). Shale gas exploration and development has sparked great interest worldwide, owing to its tremendous success in North America, and it plays a vital role in meeting rising energy needs (Shen et al. 2018),

CONTACT Khairul Azlan Mustapha azlan_0401@um.edu.my; nurayelwa@yahoo.com Department of Geology, University of Malaya, Kuala Lumpur 50603, Malaysia

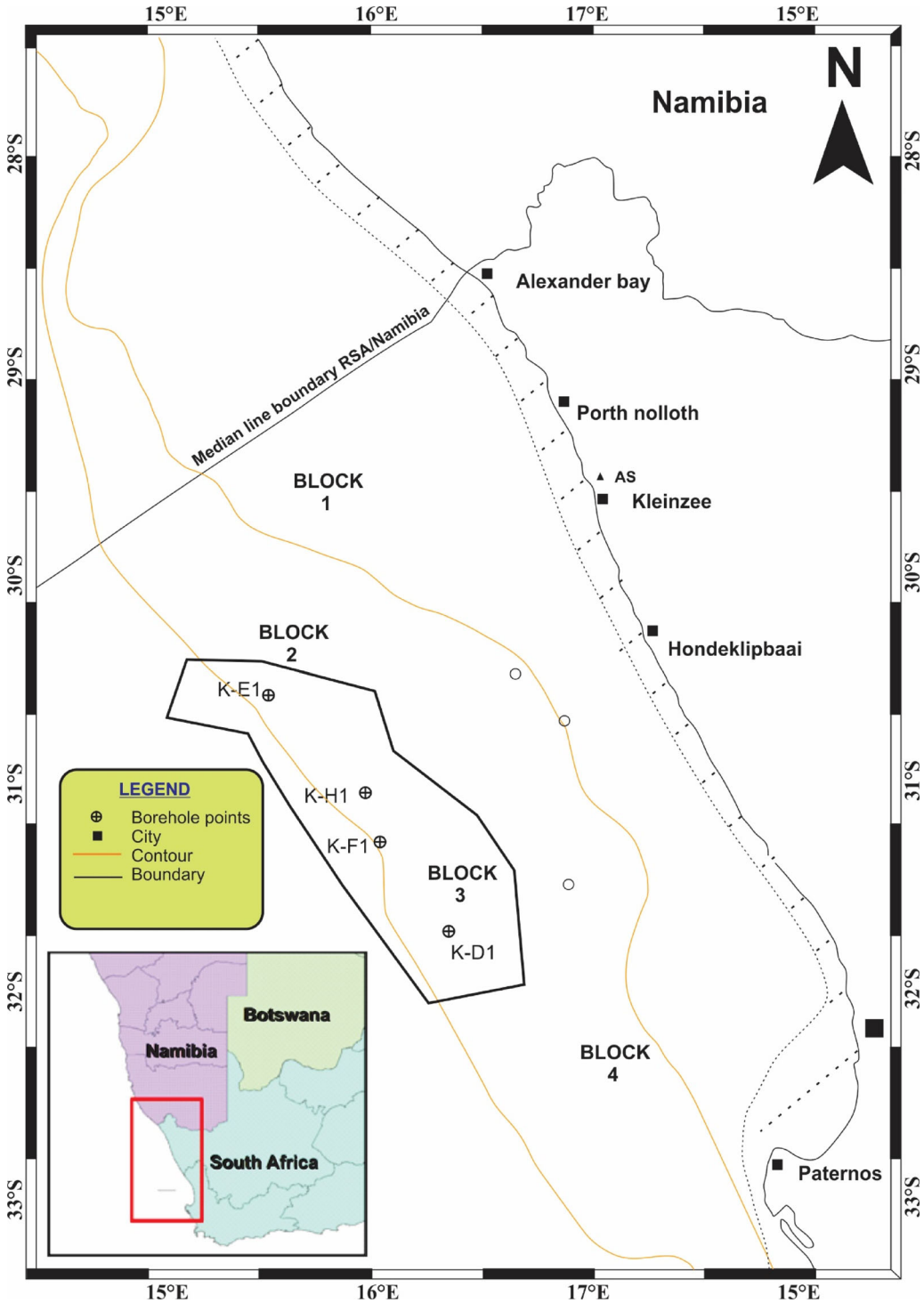

Figure 1. Locality map of boreholes and prospects of the study area, Orange Basin.

contributing over 14% of all the gas produced in the United States in 2004 (Jarvie et al. 2007). Shale gas production growth and extrapolations in the United States contributed significantly to the increase in 2012. Proven shale gas reserves have increased considerably, and total yearly gas production has grown year after year. It is expected to produce more than half of the natural gas supply by 2040 (Energy Information Administration [EIA] 2014). The Permian black shales of the Lower Ecca Group formations in the Karoo Basin are thought to be potential shale gas source rocks (Chere 2015). Most recently, the US EIA (2015) estimated a technically recoverable shale gas resource of 370 trillion cubic feet (Tcf) in the Karoo Basin (Chere et al. 2017). Unique multifactorial concerns, like shale gas prospecting, frequently have ramifications across South African governing system (Atkinson 2018; Van Huyssteen et al. 2016) which posed severe challenges in its development. Two government-funded research studies have thoroughly examined the possible effects of shale gas mining in the country (Africa 2016; Scholes et al. 2016). No unconventional shale exploitation has yet occurred

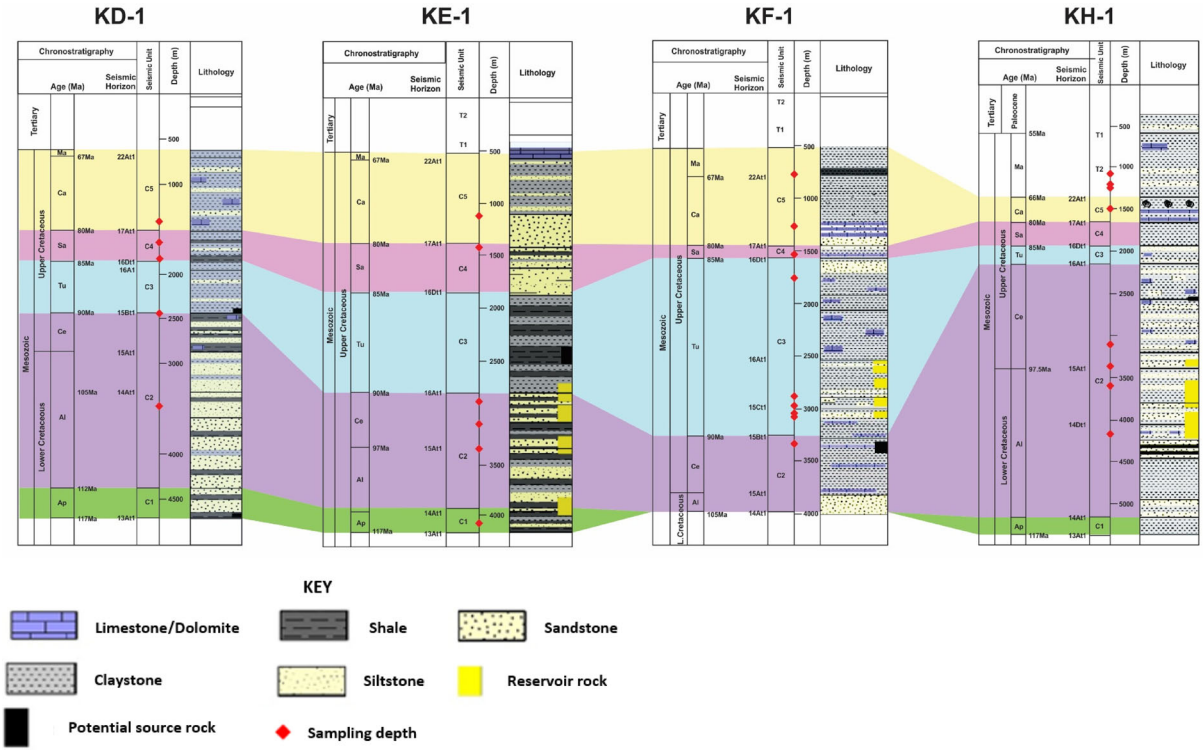

Figure 2. Generalized stratigraphic columns of the Cretaceous-Tertiary succession of selected wells in the Orange Basin based on system tracts and seismic units. The red spots indicate the sampling depths (m).

in South Africa, and gas exploration has been minimal (Atkinson 2018).

In Asia, especially China, shale gas production began in 2012 where enormous shale gas plays have been discovered (Caineng et al. 2010; Li et al. 2013; Caineng et al. 2015). Some shale plays exist throughout the Asian continent, and more new proposals are in the works to explore additional resources in emerging economies, including India and Saudi Arabia (Mustafa et al. 2022). Pakistan has about 3000 billion cubic metres of shale gas reserves (EIA 2015; Sohail, Radwan, and Mahmoud 2022). According to a World Resources Institute report, China is projected to have thirty trillion cubic metres of unutilized shale gas and is currently ranked first globally (Wang et al. 2016; Li et al. 2018). In 2013, China's proven shale gas reserves and current yearly gas generation yielded 2×10^8 m^3 of shale gas (Zhang et al. 2022). Gas production surpassed 100×10^8 m^3 in 2018. In 2020, Li et al. (2018) projected gas production to reach 2×10^{12} m^3 to 200×10^8 m^3, or even up to 300×10^8 m^3 (Caineng et al. 2015), accounting for an additional 10% of total gas yield (Zhang et al. 2022); placing China amongst the planet's most incredible shale gas volume and development. Many marine shale gas fields with reserves of 100 billion cubic metres have already been put in place in the Sichuan Basin and its outskirts, together with Fuling and Changning-Weiyuan, with the Longmaxi Formation as the primary target horizon (Zhang et al. 2022). The EIA revealed that the worldwide recoverable shale gas fields were 220.73×10^{12} m^3 (EIA 2013; Li et al. 2018).

Using non-conventional and conventional tight petroleum reservoirs with lateral multi-stage fracturing, microseismic or other techniques is more cost-effective and reliable (Bilgen and Sarikaya 2016). It can thus significantly improve oil and gas recoveries, boosting unconventional supplies of tight oil and gas in and out of conventional realms. Shale gas is essential in increasing energy production (Zhang et al. 2022). It is a suitable replacement for the steadily drained conventional petroleum proliferating in reservoirs worldwide (Li et al. 2018). Exploiting shale gas reservoirs could boost biogas yield and reduce the intensity of the unending oil shortage. Uncovering more hidden treasures accumulating in nano-sized pore spaces impacts the micro reservoir, adding different shale gas resource types and increasing global surpluses. Hence, shale gas has the potential to improve energy security and safety while lowering emissions in several regions of the world (Zhang et al. 2017).

Shale gas reserves nevertheless have low physical properties making them difficult to develop (Shen et al. 2017). The shale of the Orange Basin has been buried to enough depth in most parts of the Orange Basin to achieve oil and gas generation stages. Commercial gas resources are continually generated when shales reach the gas window (>1.0% Ro in oil). The AK wells produce gas and probably optimize the kudu gas and Ibhubesi fields in Namibia (Kuhlmann et al. 2010; Van der Spuy et al. 2003), e.g., the transitional drift tectonic phase (Van der Spuy et al. 2003). In addition, within AK1 half-graben, Turonian drifting phase source of gas and oil interval is probably like that induced in the terrestrial oil sources of the Barnet shale or Smithwick Shale hydrocarbons by mixing or variation of organo-facies (Jarvie et al. 2003). Orange Basin shales contain a good TOC (1–2% wt.), yet the initial hydrogen (<200 mg HC/g rock) index is relatively low. This result is like Smithwick Shale,

Fort Worth Basin, an outstanding petroleum source potential (Jarvie et al. 2007).

While the Orange Basin Shale is known to be organically rich, having large net shale thickness, high Type III content likely to generate gas, and responds to stimulation efforts, its unconventional hydrocarbon resource generation, resource management, storage and access is yet to be tapped. Following previous articles, the study focuses on the shale intervals of hydrocarbon generation opportunities within the Cretaceous succession from exploratory wells on the west and central shore of South Africa Orange Basin. The objective is to find out more about the Orange Basin's potentials. Geochemical and microscopic analysis were carried out in the sampling depths (Figure 2), which included 30 shale samples from 4 exploration wells in the Orange Basin (Figure 1). The goal was to look into organic matter in Cretaceous shale succession in quantity and quality and their relevance to the potential for hydrocarbon production. Using multi-geochemical techniques, we measure organic matter contents, both quantitatively and qualitatively, and microscopic visualization to assess thermal maturity stages. In addition, we discuss how the content of shale gas generation can be linked. This article expands knowledge about the definition of potential source rocks that could be used to explore and exploit conventional and unconventional hydrocarbons in the basin.

2. Geological settings

South Africa's deep-water basins are split into three tectono-stratigraphic basins: western, southern, and eastern (Jungslager 1999), which comprise the seven sedimentary basins in South Africa (McMillan et al. 1997). The west coast is a diverging passive Orange basin that evolves in Jurassic housing parallel graben and half-graben to the shoreline after splitting South America and African plate (Paton et al. 2007). From the shelf to the deep offshore sea, it is about 160,000 km^2 and varies between 31–33.5° S latitude and 16–17° E longitude (Figure 1) below aerial depths of more than 3000 m (Broad et al. 2012). Orange Basin is a famous rift-drifting, a silent volcanic margin that records the disintegration of Gondwana and the widening of the Atlantic (Hartwig, Anka, and di Primio 2012). This same basin goes all the way up to Namibia's deep water southwest eruptive fault-bounded passive continental margin (Paton et al. 2007) and nearly 43,000 km^2 of total offshore license space (Gerrard and Smith 1982). South Africa's largest deep – sea basin is the Orange Basin (McMillan et al. 1997), including a vast post-drift sequence piling off Namibia's west and south banks, containing sedimentary sequence ranging from the Late Jurassic to the Recent (Brown 1997; Petroleum Agency of South Africa and P 2003), having an accumulation thickness of about 7 km (north) to about 3 km southward (Gerrard and Smith 1982). The Orange River fills the Orange basin northern portion facing an opposing delta. In the pre-Hauterivian age, the earliest sediments were deposited, making the Western shoreline sediments continental with volcanic (Fatti et al. 1994). The volcanic intersections are contemporary with Barremian transgressive sequences that show the West Coast is volcanic in type (McMillan et al. 1997). The Orange Basin includes an inherent sequence of pre-drifting synthetics of siliciclastic and lacustrine sediments with minor volcanic rocks between Late Jurassic and Hauterivian ages and early drifting of proven and inferred rocks of Barremian-Lower Aptian sources (Paton et al. 2007).

Tertiary sediment consists of chemical deposits and limy oozes, with a thick drift block constantly deformed to the edge of the old shelf, with piled sediments and unstable slopes out in the upper cretaceous period. In this tectonic event, extensive gravity failure and a fold-up split-up stream across pressure shales were observed (Jungslager 1999). This western coast has a disjointed crustal section, with a rifted southern section (Visser et al. 1998) having continental deposits from the east towards the deep sea in the west. Approximately, 75% of the potential areas are under the 500 m water depth (Jungslager 1999). Drifting apart, the reservoir rocks consist of fluvial and deltaic sandstones with conglomerates and rocks underneath them. At the drifting stage, fluvial sandstones and floodplain sediments can be found. The Orange Basin contains a variety of plays, such as fault-bounded plays, which are lacustrine sands that also trap petroleum from carbon-containing claystones. Synrift accumulations of drift plays, including early Cretaceous aeolian sandstones and Albian incised valley play systems, structural plays through superficial sediments, and coastal waters housing rollover anticlines, are also significant (Van der Spuy et al. 2003).

3. Material and experimental techniques

Thirty shaly cuttings were obtained from four stratigraphic units of C5, C4, C3, and C2 across four boreholes, i.e., KD1, KE1, KF1, and KH1 (Figure 2). Shales under consideration were collected between 820 and 4232 m burial depths at a regular sampling interval (Figure 2). However, contaminants from drilling mud were seen in the cuttings, which were removed before geochemical analyses. Geochemical research carried out on shale samples includes; TOC analysis, rock – Eval combustion, Soxhlet extraction, microscope examinations of maceral sorts, palynofacies, and vitrinite reflectance measurements (VRo percent).

The shale samples studied for TOC (wt.%) and rock-eval pyrolysis were crushed to a mesh size less than 200 and used the pyrolysis machines LECO CS244 Carbon/Sulphur and Rock-Eval VI for the analyses. A Rock-Eval VI pyrolysing machine adapted to depict bulk composition organic matter in powdered shale samples, such as free hydrocarbon (S_1), potential HC generation (S_2), the proportion of CO_2 product of kerogen combustion (S_3), and maximum S_2 generation Tmax (C) by arbitrating plant matter abundance (Espitalié, Deroo, and Marquis 1986; Peters and Cassa 1994). Also, the hydrogen index (HI), oxygen index (OI), production yield (PY), and production index (PI) were computed based on the source rocks' organic content (Espitalié, Deroo, and Marquis 1986; Hakimi et al. 2020b; Peters and Cassa 1994).

Slandering technique was used to separate extractable materials from the analysed shale. Briefly, 5–10 g of each crushed sample was mixed in a solvent of 93% dichloromethane and 7% methanol using a Soxhlet facility for 72 h. Then, using liquid column chromatography, the extracted organic matter was differentiated into saturates, aromatics, and NSOs fragments utilizing petroleum ether, dichloromethane, or methanol. The three fractions were left behind in 3 ml vials and allowed to dry at room temperature. Finally, the dried saturate, aromatic, and polar NSO were weighed.

The studied shales were also prepared for the organic petrographic examination, including kerogen types related to the thermal maturation of the organic facies (Hackley and Cardott 2016). Maceral investigation was handled using a standard polished block preparation procedure, e.g., Taylor et al. (1998). First, the lithology has been pulverized into pea pieces (1–2 mm) and put in moulds made with Serifix resin and hardener blend. After hardening, the polish block was ground to expose the sample surface then singly polished to smoothen the surfaces with silicon carbide paper and alumina powder; initially 1 um, then 0.05 um grade using isopropyl alcohol as a lubricant. Then, organic petrographic examinations were performed applying standard white light, oil immersion, and cross polarize ultraviolet light utilizing LEICA DM6000M microscopes coupled with DISKUS fossil software, used for VR and Maceral point counting. Next, LEICA CTR 6000 photometry assembled with fluorescence illuminator where occurrence and organic matter types description of the type of kerogen was buttoned up utilizing both the regular white and infrared light.

In palynofacies analysis, each sample's wet kerogen concentrate was smeared on a slide and allowed to air dry around 25 and 30 °C. After that, the specimen slides were covered with Sigma Aldrich Canada balsam and a 24 × 32 mm coverslip for 30 min to dry. Each prepared sample on a glass slide was mounted for visual kerogen examination using LEICA CTR 6000 photometry, assembled with a fluorescent imager. The occurrence and organic matter type characterization of the type of kerogen were bundled up by employing standard white light and ultraviolet rays. Standard palynological procedures (Wood 1996) were used for evaluating kerogen quality visually. It is envisioned using a glass slide to record organic matter diversity and compute its percentage abundance. Such observations allowed for the inspection of the kerogen content and category of hydrocarbons produced throughout maturation.

4. Results

4.1. Borehole correlation

Borehole logging was effective in identifying the various lithofacies. As shown in Figure 2, the lithologic log data used to describe the lithological units of the studied samples were extracted from actual drilling results and prognostic features. These were related to the already established seismic horizons. No detailed stratigraphic classification was undertaken as beyond the scope of the research. This section presents the stratigraphy of the KD1, KE1, KF1, and KH1 well logs to highlight the primary rock units.

KD-1 well generally comprises claystone with shell fragments, limestone and dolomite stringers, shallow marine sandstone, and siltstones. In the Turonian-Santonian lower successions, the claystone grades to massive shales. Shales are intercalated with siltstone having minor limestone, dolomite, and sandstone in shallow and deeper places.

In the KE-1 log, in the uppermost succession coexists limestone with abundant shell debris. This upper post-rift succession houses sandstone stringers that are slightly thicker and more extensive. Claystone are sub-fissile, darker grading to siltstone in some places during the Santonian to Carboniferous era. Shaly sandstone and siltstone are underneath. During Turonian, within the lower post-rift package lies interbedded shale with claystone. Sandstone is thinly interbedded with claystone. Deeper Aptian to Albian sequence consists of black fissile shale and brownish-grey claystone intercalated with argillaceous siltstone.

KF1 well, on the other hand, comprises shelly and slightly glauconitic clays spanning from Carboniferous *via* Maastrichtian. The clays are non-calcareous, having pebbles, silty lignite fragments-limestone stringers with thin moderately sorted sandstone in between. Limestone with fossil stringers is shared within the upper post-rift succession-massive claystone succession with calcarenite stringers at the top with quartz traces within the Santonian era. The lower sediments have claystone, which is non-calcareous, sticky to blocky, very slightly carbonaceous, pyritic, and silty clays. Massive claystone with prominent sandstone at the upper part. Limestone's are rare, but dolomite stringers are common. A massive claystone interval with plenty of dolomite stringers was increasingly becoming arenaceous with depth from Cenomanian to Turonian.

In the KH-1, claystone interval has subordinate sandstone intercalated with limestone and dolomite stringers, commonly at shallow surfaces. Within the lower post-rift succession lies abundant non-calcareous claystone, slightly carbonaceous with few pyritic intervals having minor siltstone. Rare sandstone and dolomite stringers occur. Intercalated sandstone, siltstone, and claystone intervals were observed. Dolomite stringers are present intermittently during the Cenomanian. Massive claystone with minor siltstone, sandstone interbeds, and occasional dolomitic stringers were observed towards the Albian. A thin sandstone layer extensively separates a huge claystone sequence from Aptian to Albian track.

4.2. Organic petrological examinations

The quantitative maceral composition was assessed microscopically to characterize the examined sediments' kerogen types. Microscopic observations show that the examined samples have three macerals rich in clay minerals (Vitrinite, Inertinite, and Liptinite) as shown in photomicrographs (Figure 3). The maceral composition was determined based on mineral matter and mineral matter free (Table 1). The shale samples are entirely dominated by mineral matter between 24.00 and 69.00%. On the contrary, the disseminated primal matter is mixed with many pyrite and clay

a) KF1-3305.Normal white light
b) KF1-3305 pale green ring agglomerated sporinite (sp)
c) KD1-1370. Normal white light
d) KD1-1370. Pale yellow cutinite (ct)
e) KD1-3120. Normal white light where desmocolinite, clay and little resinite seen
f) KD-1 3120 Non-fluorescence macerals
g) KH1-3080. Bands of vitrinitic materials
h) Vitrinite under ultraviolet light where the cell wall (cw) glows to green color owing to incorporation of resinous and non-resinous materials

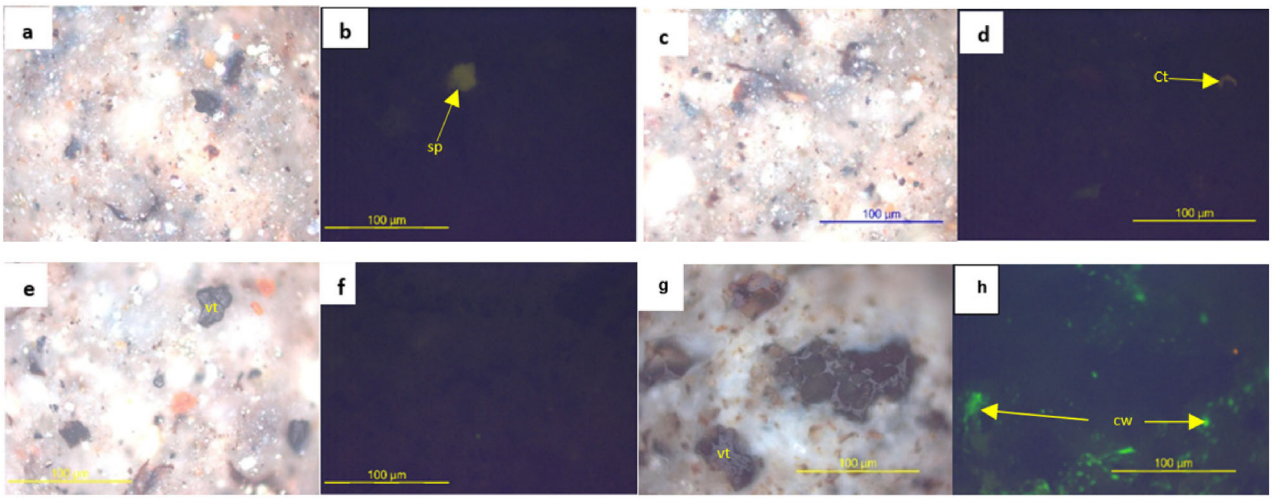

Figure 3A. Photomicrograph of maceral phytoclast under reflected white light and UV light using polish block shale samples.

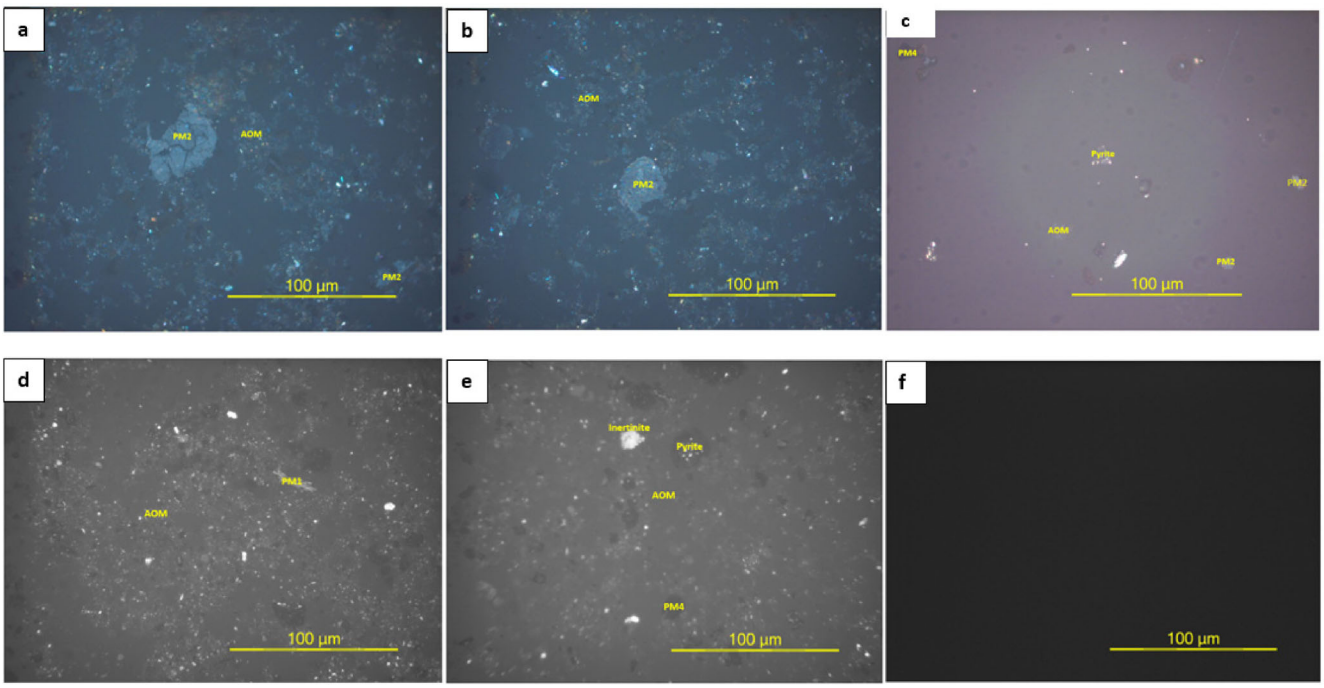

Figure 3B. Photomicrographs of recognized palynofacies phytoclast subgroups (PM1, PM2, and PM4) and amorphous organic matters (AOM) using glass slides in reflected light (a)–(e) and ultraviolet (UV) light (f).

minerals. Concerning mineral matter free, the shale samples also have a high abundance of the vitrinite maceral, ranging from 63.64 to 89.58%. Inertinite macerals have a moderate to high occurrence with a range of 8.33–31.82%, whereas liptinite macerals are less common or virtually absent (0.0–8.33%) (Figure 3(A)). The amount of gas-prone Type III aromatic hydrocarbons is more significant due to the presence of more than 60% Vitrinite maceral in such shales (Table 1; Figure 8(B)) than the majority of those other oil-prone liptinite maceral classes. Additional visual kerogen

Table 1. Petrographic analysis of the analyzed shale samples from exploration well location in the West coast of Orange Basin, South Africa covers of Vitrinite reflectance (VR_o %) and maceral counting percentage along with basis of mineral matter (vol. %) and mineral-matter-free (vol. %)

Well depth (m)	Age	Seismic units	%VRo	Maceral composition (%)			Mineral matter %	Maceral composition (free minerals %)		
				Liptinite	Vitrinite	Inertinite		Liptinite	Vitrinite	Inertinite
KE1-1250	Campanian	C5	0.58	0	27	4	69	0.00	87.10	12.90
KE1-1480	Lower Campanian	C5	0.68	0	32	7	61	0.00	82.05	17.95
KD1-1370	Santonian	C4	0.57	3	27	6	64	8.33	75.00	16.67
KH1-1500	Coniacian	C3	0.56	2	28	14	56	4.55	63.64	31.82
KD1-1650	Coniacian	C3	0.58	0	63	13	24	0.00	82.89	17.11
KD1-1900	Coniacian	C3	0.56	0	53	8	39	0.00	86.89	13.11
KD1-2250	Upper Turonian	C3	0.54	0	60	14	26	0.00	81.08	18.92
KE1-2970	Upper Turonian	C3	0.75	3	60	9	28	4.17	83.33	12.50
KH1-3080	Upper Cenomanian	C2	0.80	0	49	6	45	0.00	89.09	10.91
KE1-3110	Upper Cenomanian	C2	0.56	0	51	6	43	0.00	89.47	10.53
KH1-3350	Mid Cenomanian	C2	0.90	1	46	13	40	1.67	76.67	21.67
KH1-3510	Mid Cenomanian	C2	0.71	1	51	8	40	1.67	85.00	13.33
KF1-3305	Lower Cenomanian	C2	1.01	3	45	6	46	5.56	83.33	11.11
KD1-3120	Upper Albian	C2	0.87	2	52	5	41	3.39	88.14	8.47
KE1-3340	Upper Albian	C2	0.79	1	43	4	52	2.08	89.58	8.33
KE1-4105	Upper Aptian	C2	0.85	0	47	6	47	0.00	88.68	11.32

typing is included in the maceral data analysis to support claims about organo-facies features (Hakimi et al. 2020c) (Figures 3(B) and 8(A)). Visual examination reveals a high preponderance of AOM (more than 80%) in the kerogen concentrate of all evaluated samples (Figure 3(B)). The AOM identified in the examined samples is classified based on (Mustapha 2016; Suarez-Ruiz et al. 2012) as the non-fluorescent, structureless type that appears as brown-ash and frequently has pyrite fragments (Figure 3(B)); principally of Type III kerogen. The existence of non-glowing AOM from shallow to deeper depths could be due to rapid degeneration of woody terrestrial tissues and the fragmentation of vitrinite or inertinite macro-elements (Adegoke 2015; Largeau and De Leeuw 1995; Sawada 2006).

The vitrinite maceral is mostly brittle with an angular surface and diverse forms, according to optical properties using white light reflected. As a result, the matrix looks greyish and moderately portrayed in various forms (Figure 3(A(a, c, e, and g)). In addition, UV-light excitation was mainly used to distinguish between liptinite assemblages and shows that the liptinites appear low reflectance under normal white light and intensifying structural attributes among the few that fluorescence. The minor liptinitic maceral that faintly fluoresces includes resinite, cutinite, and sporinite in decreasing abundance and are characterized by fluorescence intensities ranging from greenish to yellow (Figure 3(A(b, d, f, and h)). However, the substantial vitrinitic maceral is followed by inertinite and discrete liptinite materials exhibiting kerogen of Type III (Mustapha and Abdullah 2013).

In all samples analysed, VRo was measured and presented in Tables 1 and 4. The Vitrinite maceral does have a modest reflectivity that tends to increase with thermal maturation. As a result, it is attributed to the high burial heat from its hosted rock formations. Therefore, percent VRo is an important measure for establishing organic carbon maturity. A key measure providing information about the maturity of plant material is VRo (Sweeney and Burnham 1990; Teichmüller, Taylor, and Littke 1998), commonly used as evidence of maturity (Hakimi, Al-Matary, and Hersi 2018; Jarvie et al. 2007; Osli, Shalaby, and Islam 2018; Shalaby, Hakimi, and Abdullah 2011). Each sampling unit received about 30 VRo readings in this study, avoiding reworked vitrinitic materials and inter-maceral effects (Teichmüller, Taylor, and Littke 1998) (Tables 1 and 4).

4.3. Total organic carbon composition and Soxhlet extraction

TOC composition is evaluated mainly as weight % and is widely used to indicate organic matter and oil generating capacity during maturity (Jarvie and Lundell 1991; Peters and Cassa 1994). TOC consists of two components; one section produces hydrocarbons upon thermal maturity, while the other is non-generative carbon (NGOC) (Cooles, Mackenzie, and Quigley 1986). Intense heat cracks the generative organic carbon (GOC) into lighter oils, gases, pyro-bitumen hydrocarbons, and pyro-bitumen by increasing temperature and maturation conditions. On the other hand, only a few gases are produced by the NGOC (Jones 1984). However, they can act as a sorbate and a catalytic converter. In addition, NGOC is used to calculate the kerogen density, which is denser and more condensed with lower hydrogen concentrations. Therefore, most geochemists argue that sediments with a TOC content of more than 1% indicate good potential for hydrocarbon generation (Bissada 1982; Katz and Lin 2014).

The analysed lithology is of average quality to relatively good TOC content between 0.80 and 1.97 wt.%, as shown in Tables 2–4. Of the 28 investigated samples, 22 have TOC content of more than 1% (1.06–1.97 wt.%); the other six samples have the lowest TOC values between 0.80 and 0.98 wt.%. In essence, most explored shales are good source rock at optimal thermal maturity levels, and they can contribute to petroleum generation. Furthermore, the quantity of free bitumen extracted was measured in the examined samples ranging between 482 and 2991 ppm (Table 3) as in line with the TOC content, which further suggests fair to high-quality source rock potential. Also, bulk constituents for extracted bitumen are measured and reported in Table 3, comprising saturated, aromatic hydrocarbons, and NSO

Table 2. Geochemical results of TOC, bulk Rock-Eval pyrolysis of the analysed shale samples from **S_2X100/TOC** exploration well location in the West coast of Orange Basin, South Africa

				Bulk rock-Eval pyrolysis								
Well-depth (m)	Age	Seismic units	TOC wt%	S_1 mg HC/g	S_2 mg HC/g	S_1+S_2 mg HC/g	S_3 mg CO_2/g	S_2/S_3	Tmax °C	HI S_2*100/ TOC	OI S_3*100/ TOC	PI mg HC/g
KFI 820	Campanian	C5	0.82	0.49	0.92	1.41	2.43	0.38	470	112	296	0.35
KE1-1250	Campanian	C5	1.24	0.08	0.52	0.60	1.54	0.34	428	42	124	0.13
KFI 1385	Campanian	C5	0.98	0.48	1.28	1.76	4.51	0.28	473	131	460	0.27
KE1-1480	Campanian	C5	1.17	0.06	0.47	0.53	1.49	0.32	429	40	127	0.11
KD1-1370	Santonian	C4	0.93	0.16	0.61	0.77	1.42	0.43	425	66	152	0.21
KFI 1525	Santonian	C4	0.92	–	–	–	–	–	–	–	–	–
K-FI 1565	Santonian	C4	1.12	0.52	1.41	1.93	2.28	0.62	464	126	204	0.27
KHI-1170	Coniacian	C3	1.10	–	–	–	–	–	–	–	–	–
KHI-1360	Coniacian	C3	0.80	–	–	–	–	–	–	–	–	–
KHI-1380	Coniacian	C3	1.12	–	–	–	–	–	–	–	–	–
KH1-1500	Coniacian	C3	0.91	0.36	0.9	1.26	2.14	0.42	443	99	235	0.29
KD1-1650	Coniacian	C3	1.06	0.26	1.12	1.38	1.32	0.85	427	106	125	0.19
KD1-1900	Coniacian	C3	1.19	0.18	1.08	1.26	1.45	0.74	425	91	122	0.14
KD1-2250	Upper Turonian	C3	1.68	0.19	1.26	1.45	1.5	0.84	426	75	89	0.13
KE1-2970	Upper Turonian	C3	1.43	0.16	1.02	1.18	1	1.02	427	71	70	0.14
KFI-2825	Upper Cenomanian	C2	1.97	–	–	–	–	–	–	–	–	–
KH1-3080	Upper Cenomanian	C2	1.43	0.41	1.81	2.22	2.08	0.87	438	127	145	0.18
KE1-3110	Upper Cenomanian	C2	1.22	0.13	0.8	0.93	1.12	0.71	430	55	92	0.14
KF1-2975	Mid Cenomanian	C2	1.8	0.3	1.5	1.8	–	–	–	85	–	0.17
KF1-3035	Mid Cenomanian	C2	1.44	0.2	1.10	1.30	–	–	–	102	–	0.15
KF1-3055	Mid Cenomanian	C2	1.73	0.4	1.6	2	–	–	–	109	–	0.71
KH1-3350	Mid Cenomanian	C2	1.20	0.48	1.59	2.07	2.04	0.78	430	133	170	0.23
KH1-3510	Mid Cenomanian	C2	1.29	0.55	1.71	2.26	2.24	0.76	469	133	174	0.24
KF1-3305	Lower Cenomanian	C2	1.46	0.47	1.45	1.92	1.8	0.81	460	99	123	0.24
KD1-3120	Upper Albian	C2	1.55	0.26	1.36	1.62	0.67	2.03	434	88	43	0.16
KE1-3340	Upper Albian	C2	1.89	0.23	1.41	1.64	1.95	0.72	435	75	103	0.14
KH1-4232	Upper Albian	C2	1.48	0.3	1.21	1.51	1.32	0.92	476	82	89	0.20
KE1-4105	Upper Aptian	C2	1.21	0.29	0.97	1.26	1.23	0.79	439	80	102	0.23

Table 3: Bitumen extractions and their compositions (i.e., aliphatic, aromatic and NSO) characteristics and their contributions to petroleum generation potential

Well-depth (m)	Age	Seismic units	wos(g)	extract/oil (g)	YE	EOM (ppm)	TOC wt%	Aliphatic (wt%)	Aromatic %	NSO %	CNE	CNH	Sats/Arom (g)
KFI 820	Campanian	C5	5.032	0.0116	2.305	2305	0.82	1.7	12.1	86.20	281.128	38.796	0.1405
KE1-1250	Campanian	C5	4.99	0.0036	0.720	720	1.24	27.8	11.1	61.10	58.104	22.602	2.505
KF1-1385	Campanian	C5	4.95	0.0067	1.354	1354	0.98	4.5	6	89.6	138.183	14.509	0.75
KE1-1480	Campanian	C5	4.98	0.0024	0.482	482	1.17	29.2	8.3	62.5	41.19371	15.448	3.518
KD1-1370	Santonian	C4	4.97	0.0034	0.683	683	0.93	8.8	32.4	58.8	73.430	30.253	0.272
KFI 1525	Santonian	C4	5.02	0.0056	1.1150	1115	0.92	3.57	7.14	89.3			0.50
KFI 1565	Santonian	C4	5.08	0.003	0.590	590	1.12	33.3	16.7	50	52.683	26.3417	1.994
KH1-1170	Coniacian	C3	4.99	0.0059	1.1815	1182	1.10	15.25	16.95	67.80			0.9000
KH1-1360	Coniacian	C3	5.1069	0.0054	1.1000	1057	0.80	27.27	12.12	60.61			2.25
KH1-1380	Coniacian	C3	5.0208	0.0074	1.4739	1474	1.12	3.17	9.52	87.30			0.3329
KDI-1650	Coniacian	C3	5.02	0.0043	0.856	856	1.06	11.6	9.3	79.1	80.740	16.875	1.247
KD1-1900	Coniacian	C3	5.01	0.0071	1.417	1417	1.19	4.2	4.2	91.5	119.100	10.004	1
KD1-2250	Upper Turonian	C3	4.99	0.003	0.600	601	1.68	13.3	13.3	73.3	35.770	9.5148	1
KE1-2970	Upper Turonian	C3	4.99	0.0034	0.682	682	1.43	20.6	20.6	58.8	47.658	19.635	1
KH1-3080	Upper Cenomanian	C2	4.95	0.010	2.041	2041	1.43	3	3	94	142.697	8.56183	1
KE1-3110	Upper Cenomanian	C2	5.02	0.0029	0.578	578	1.22	10.3	6.9	82.8	47.355	8.1451	1.493
KF1-2825	Upper Cenomanian	C2	4.53	0.0076	1.6762	1676	1.97	15.79	10.53	73.68			1.500
KF1-2975	Mid Cenomanian	C2	5.01	0.016	3.274	1477	1.8	2.7	5.41	91.89	181.880	14.750	0.499
KF1-3035	Mid Cenomanian	C2	4.98	0.011	2.270	2269	1.44	8.85	5.31	85.84	157.575	22.313	1.667
KF1-3055	Mid Cenomanian	C2	5.05	0.015	2.991	2991	1.73	7.95	6.62	85.43	172.883	25.189	1.201
KH1-3350	Mid Cenomanian	C2	4.967	0.011	2.195	2195	1.2	9.2	9.2	81.7	182.903	33.654	1
KH1-3510	Mid Cenomanian	C2	5.02	0.0086	1.714	1714	1.29	10.5	8.1	81.4	132.855	24.711	1.296
KF1-3305	Lower Cenomanian	C2	4.98	0.0067	1.347	1347	1.46	11.9	17.9	70.1	92.233	27.485	0.665
KD1-3120	Upper Albian	C2	4.99	0.0035	0.701	701	1.55	8.6	14.3	77.1	45.242	10.360	0.6014
KE1-3340	Upper Albian	C2	4.96	0.0046	0.927	682	1.89	15.2	28.3	56.5	49.0659	21.344	0.537
KH1-4232	Upper Albian	C2	5.035	0.005	1.013	1013	1.48	5.88	5.88	88.24	68.4303	8.0474	1
KE1-4105	Upper Aptian	C2	4.96	0.0028	0.564	564	1.21	17.9	10.7	71.4	46.61663	13.332	1.673

YE: Yield of extract (mg/g) = (mass of extract/mass of rock) *1000
CNE Carbon Normalized Extract= (Extract/TOC) mgHC/gTOC
Carbon Normalized HC (mgHC/gTOC)= (Sats/Arom)/TOC=====((Sats + Aro)/100)*CNE

polar. The pattern of the bulk composition shows NSO polar more prevalent with a volume of 50–94%. The notable amount of aromatic hydrocarbons is also present in the range of 3.0–32.4% volume, followed by relatively low amounts of saturated hydrocarbon (1.7–33.3%). However, the large volumes of NSO contents are due to either low

Table 4: Geochemical outcome of Rock eval pyrolysis data, thermal maturation parameters and major oxides in relation to petroleum generation potential within Orange Basin

						Chemostratigraphic variation of major oxides (%) within Orange Basin								
Well-depth (m)	Age	Seismic units	TOC wt%	S_1(b)	S_2(b)	Tmax °C	VR_O	SiO_2 (%)	Al_2O_3 (%)	Fe_2O_3 (%)	CaO (%)	MgO (%)	P_2O_5 (%)	BaO (%)
KFI 820	Campanian	C5	0.82	10.73	20.14	470	1.27	51.01	12.33	11.54	8.95	3.70	0.21	0.43
KE1-1250	Campanian	C5	1.24	1.75	11.38	428	0.58	56.56	14.35	11.57	5.02	3.54	0.19	0.05
KFI 1385	Campanian	C5	0.98	10.51	28.02	473	1.37	54.74	14.61	13.36	2.57	3.37	0.16	0.04
K-E1 1480	Campanian	C5	1.17	1.31	10.29	429	0.68	52.66	13.33	11.28	11.81	3.15	0.21	0.04
KD1-1370	Santonian	C4	0.93	3.50	13.35	425	0.57	56.72	15.2	11.55	4.38	2.79	0.24	0.06
KFI 1525	Santonian	C4	0.92	–	–	–	1.11	55.87	15.13	11.47	1.75	3.19	0.15	0.11
K-FI 1565	Santonian	C4	1.12	11.38	30.86	464	1.11	55.70	14.38	10.87	5.12	3.12	0.19	0.06
KHI-1170	Coniacian	C3	1.10	–	–	–	0.78	56.32	14.80	12.08	4.67	3.00	0.18	0.03
KHI-1360	Coniacian	C3	0.80	–	–	–	0.86	59.16	14.36	10.98	2.86	2.91	0.17	0.05
KHI-1380	Coniacian	C3	1.12	–	–	–	0.85	58.51	15.25	12.06	2.38	2.98	0.18	0.04
KH1-1500	Coniacian	C3	0.91	7.88	19.70	443	0.86	57.31	15.44	11.44	3.70	2.82	0.18	0.04
KD1-1650	Coniacian	C3	1.06	5.69	24.52	427	0.58	54.58	14.77	10.86	8.96	2.28	0.38	0.07
KD1-1900	Coniacian	C3	1.19	3.94	23.64	425	0.56	58.98	17.24	9.60	2.53	2.22	0.19	0.12
KD1-2250	Upper Turonian	C3	1.68	4.16	27.58	426	0.54	60.26	17.47	9.17	2.02	2.09	0.15	0.05
KE1-2970	Upper Turonian	C3	1.43	3.50	22.33	427	0.75	63.31	16.08	7.74	2.69	1.96	0.14	0.08
KFI-2825	Upper Cenomanian	C2	1.97	–	–	–	0.92	57.51	17.67	12.61	1.90	2.04	0.26	0.06
KH1-3080	Upper Cenomanian	C2	1.43	8.97	39.62	438	0.80	58.48	16.83	9.74	1.85	2.24	0.17	0.44
KE1-3110	Upper Cenomanian	C2	1.22	2.85	17.51	430	0.72	62.19	15.34	7.97	4.92	1.97	0.18	0.07
KF1-2975	Mid Cenomanian	C2	1.80	6.57	32.84	–	0.95	–	–	–	–	–	–	–
KF1-3035	Mid Cenomanian	C2	1.44	4.38	24.08	–	0.89	60.50	17.91	9.47	1.65	1.99	0.16	0.05
KF1-3055	Mid Cenomanian	C2	1.73	8.76	35.02	–	0.90	–	–	–	–	–	–	–
KH1-3350	Mid Cenomanian	C2	1.20	10.51	34.81	430	0.90	59.19	15.74	8.47	2.58	2.20	0.13	1.10
KH1-3510	Mid Cenomanian	C2	1.29	12.04	37.43	469	1.34	61.08	15.09	8.03	1.90	2.07	0.15	0.93
KF1-3305	Lower Cenomanian	C2	1.46	10.29	31.74	460	1.01	57.21	16.77	11.14	2.29	2.25	0.21	0.41
KF1-3345	Lower Cenomanian	C2	–	–	–	–	1.53	–	–	–	–	–	–	–
KF1-3726	Lower Cenomanian	C2	–	–	–	–	1.63	–	–	–	–	–	–	–
KD1-3120	Upper Albian	C2	1.55	5.69	29.77	434	0.87	62.46	17.85	8.04	1.56	1.97	0.14	0.05
KE1-3340	Upper Albian	C2	1.89	5.03	30.86	435	0.79	59.51	16.76	10.56	2.07	2.17	0.17	0.10
KH1-4232	Upper Albian	C2	1.48	6.57	26.49	476	1.24	60.71	16.90	9.14	1.29	2.03	0.141	0.17
KE1-4105	Upper Aptian	C2	1.21	6.35	21.23	439	0.85	61.45	16.53	9.68	2.28	2.01	0.19	0.50

S1 (b): Oil in Rock from S1 (bbl oil/ac-ft)
S2 (b): Generation Potential from S2 (bbl oil/ac-ft)
Conversion factor for S1 or S2 to bbl oil/ac-ft = *21.89

maturity, or large amounts of plant inputs in the shale sample analysed (Peters, Peters, et al. 2005).

4.4. Rock-Eval pyrolysis

Rock pyrolysis was also used to examine 23 shales. These results indicate that free petroleum exists (S_1) and petroleum generated *via* kerogen heat cracking (S_2) yields 0.06–0.55 and 0.47–1.81 mg HC/g rock, respectively (Table 2). Its S_1 and S_2 yields connotes that most samples have reasonable potential for hydrocarbon generation, even though the shaly samples are from good to very good source rocks, as evident from the relationship between the TOC and PY data in Figure 4. The S_1 product is adapted to determine the nature of the organic phase, either indigenous or non-indigenous (Hakimi, Al-Matary, and Hersi 2018; Shalaby, Hakimi, and Abdullah 2012). The low S_1 yield values indicate that the samples possess indigenous organic matter, as shown in Figure 5. The petroleum yields of S_2 and S_3 are also compatible with TOC content and imply that the analysed shales have HI and OI variables, specifically 40–133 mg HC/g TOC and 43–235 mg CO_2/g TOC, respectively (Table 2). Most samples examined ($n = 15$) have OI >100 mg CO_2/g TOC; the remaining five samples have the lowest OI value between 43 and 92 mg CO_2/g TOC. Fourteen of the shales range between 40 and 99 mg HC/g TOC for HI value, whereas the other nine samples have an HI > 100 mg HC/g TOC. This typically characterizes kerogen Type III prevalence ascertaining to expel gas as affirmed by

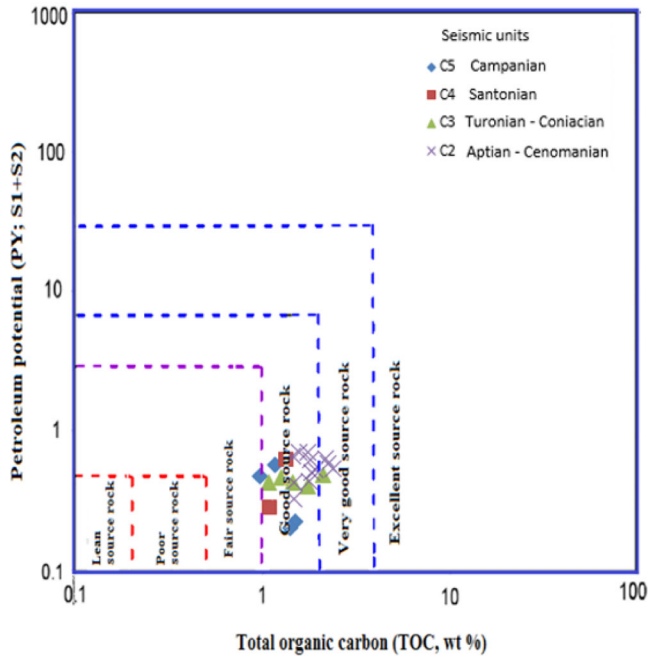

Figure 4. Geochemical comparison between total organic matter (TOC) content and petroleum potential yield ($S_1 + S_2$), illustrating that the shaly samples are from good to very good potential source rocks.

S_2/S_3 up to 1.00 mg HC/g rock. Using the Rock-Eval pyrolysis scope, T_{max} and PI values were measured from 425 to 476 °C and from 0.11 to 0.71 (Table 2).

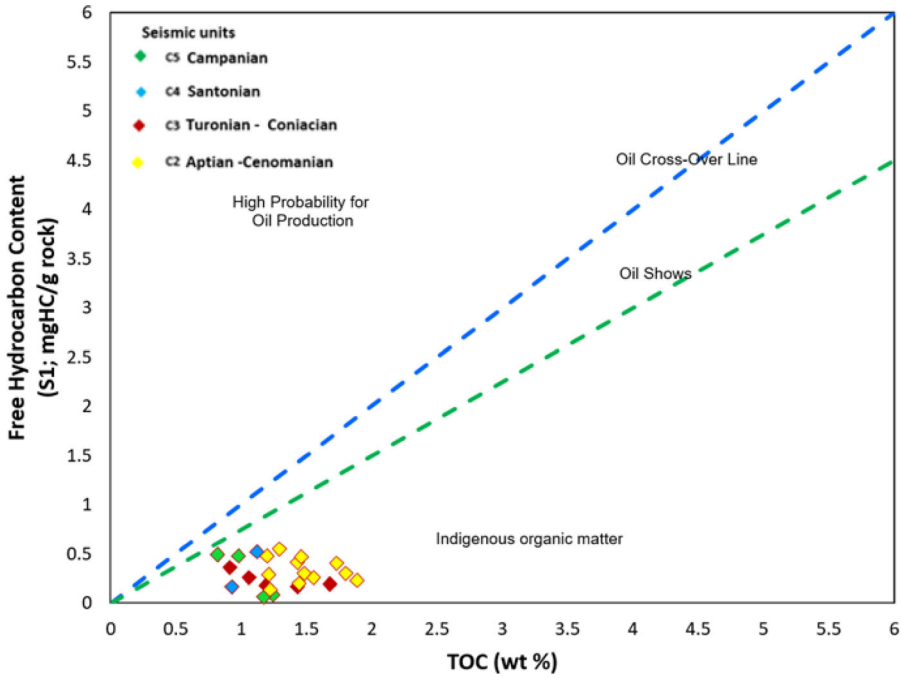

Figure 5. Plot of S_1 against TOC (wt.%) showing low probability for Oil Production.

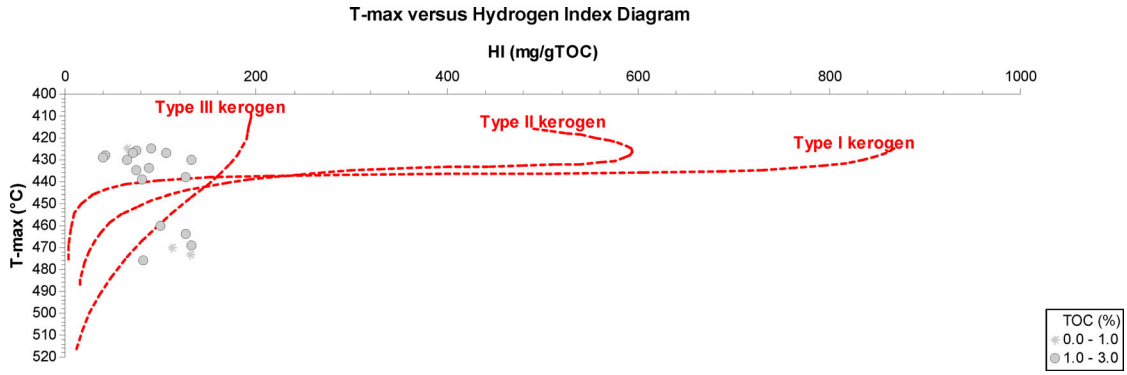

Figure 6A. Characteristics of kerogen in the Western coast within the studied 4 wells based on Rock-Eval hydrogen index (HI) *versus* T_{max} diagram.

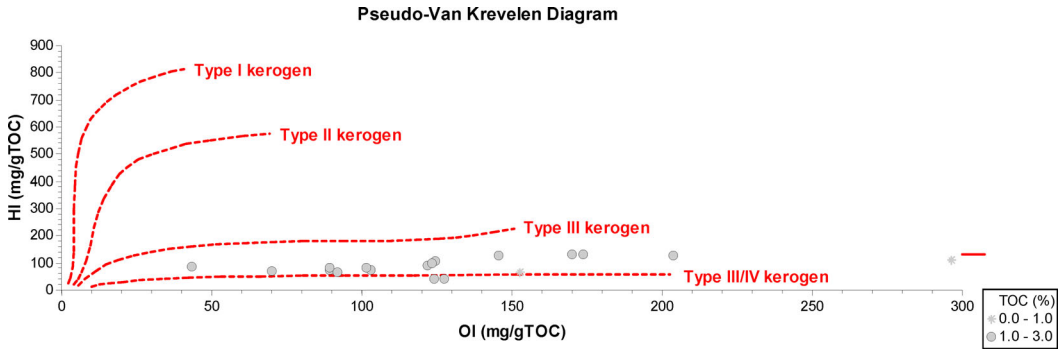

Figure 6B. Characteristics of kerogen within the Orange basin studied sediments based on Rock-Eval hydrogen index (HI) and Oxygen index (OI).

5. Discussion

5.1. Characterizing organic matter and their contributions to kerogen type

The origin of both organic sediments and their properties largely evaluates the feasibility of source rocks and their oil and gas utilization. Therefore, the distinctive kerogen typing in the studied samples was mainly determined by several quantitative and qualitative thermal decomposition analysed data combined with optical microscopy of kerogen abundances. This integration allowed us to assess the attributes and compositions of kerogen types and understand the source of organic matter, thereby predicting the most probable source of oil or gas from such sediment.

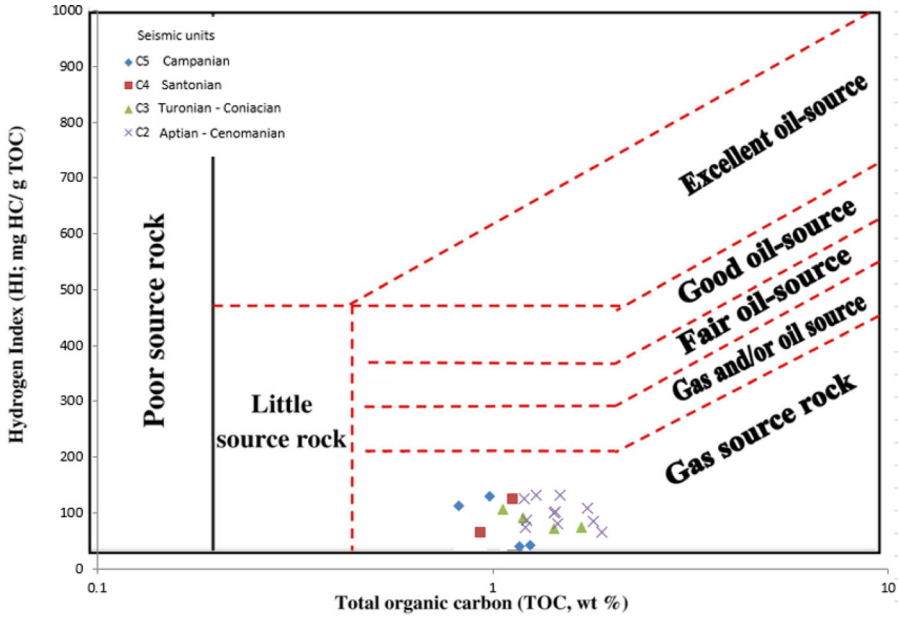

Figure 6C. Cross plot of rock eval hydrogen Index and total organic content (TOC, wt.%) indicating the hydrocarbon potential of the investigated samples.

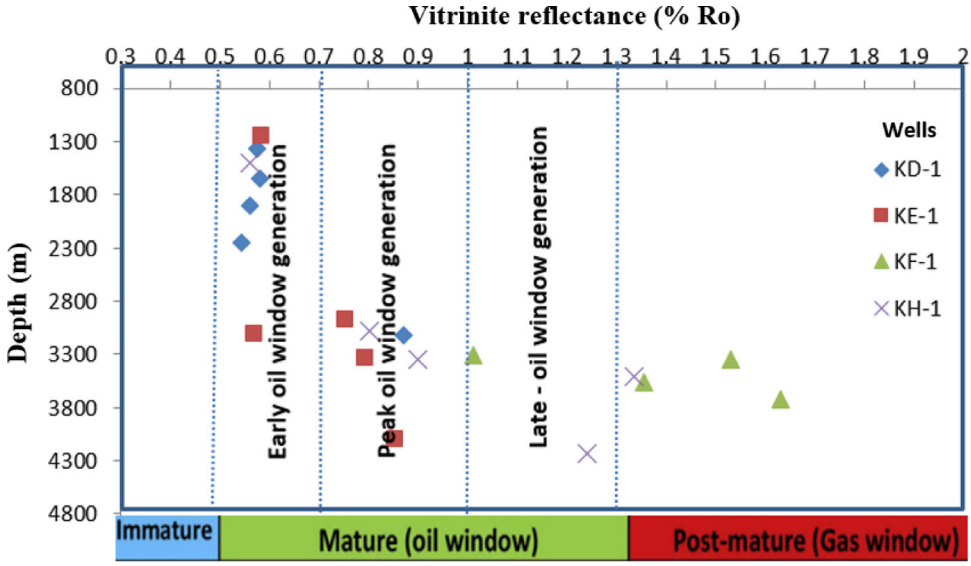

Figure 7A. Cross-plot of Vitrinite reflectance (% Ro) *versus* depth to demonstrate the distribution of the parameter with increasing depth.

The Rock-Eval HI values are used to classify datasets into the bulk kerogen qualitative category (Espitalie, Deroo, and Marquis 1985; Mukhopadhyay, Wade, and Kruge 1995; Peters and Cassa 1994). The test results had HI values less than 200 mgHC/g TOC (Table 2), inferring that they are all gas-driven shale. Rock-Eval HI, OI, and maximum temperature value plot points also supported this finding since the diagrams of van Krevelen showed that the shale samples under examination are majorly Type III, with limited Type IV kerogen (Figure 6(A,B)).

Furthermore, the maceral analysis data provides visual kerogen typing and is used to support claims about organofacies characteristics (Hakimi et al. 2020a). According to the reflected light microscopic examination, most of the analysed shales contained high vitrinitic materials with low fluorescence liptinite organic matter (Figure 3). Hence, the primary kerogen type is Type III due to more than 60% vitrinite maceral in these shales (Table 1).

5.2. Organic matter thermal maturation

The amount of heat and time required converting sedimentary matter into oil and gas is referred to as thermal maturity (Mustapha 2016; Peters and Moldowan 1993). Organic materials' maturity is determined by how much OM is heated and transmogrified into petroleum. Its evaluation is critical to the effect of heat on sediment burial, indicating the highest paleo-temperature of the source rock and identifying petroleum generation potential (Figure 7(A–E)). The principal by which a substantial percentage of petroleum is created from kerogen in source rocks is systematic diagenesis, heat maturation, or catagenesis (Hunt 1995). Under

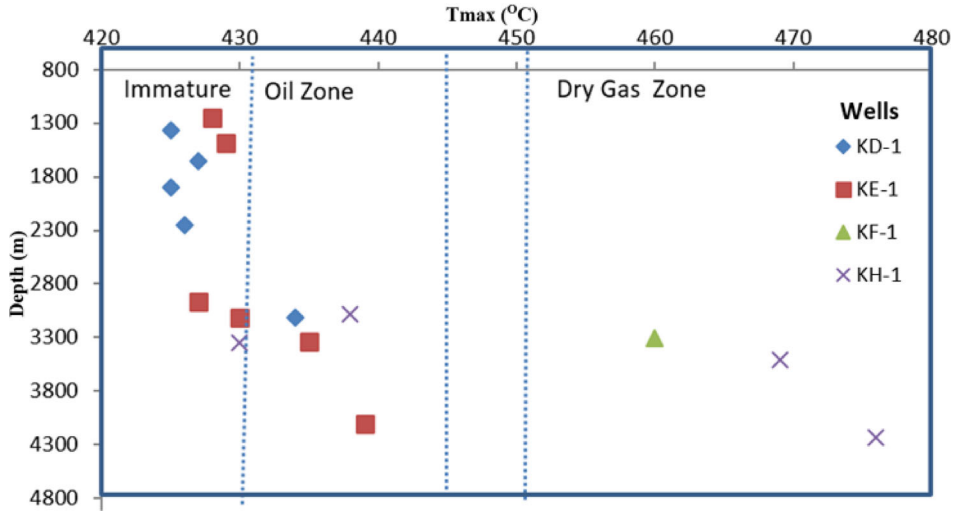

Figure 7B. Cross-plot of maximum pyrolysis temperature (T_{max}) *versus* depth.

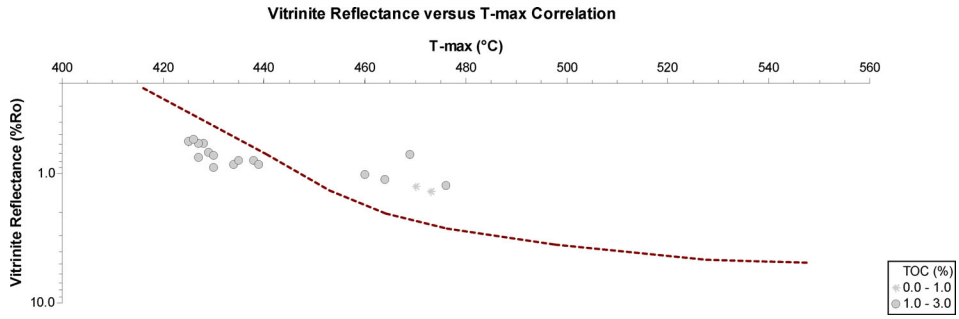

Figure 7C. Vitrinite Reflectance *versus* T_{max} correlation.

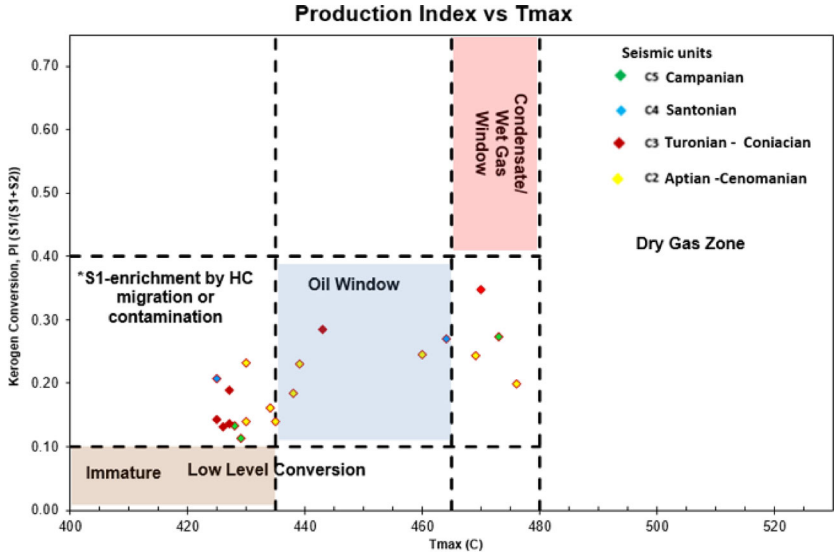

Figure 7D. Production Index *versus* T_{max} showing kerogen conversion potential.

anoxic conditions, the thermal degeneration of kerogens generates oil at temperatures of around 60–160 °C and at higher than 160 °C, it yields gas (Hunt 1995). It is an essential geochemical criterion for determining the probability of a source rock's maturity to the point where it can transform kerogen to produce petroleum (Jarvie et al. 2007; Welte and Tissot 1984). There are two primary approaches to this process: visual and chemical. Organic microscopy results, rock eval maximum temperature (°C), productive index (PI), and biomarker aspects like the plot of Pr/n-C_{17} *versus* Ph/n-C_{18}, C_{32} homohopane proportion (22S/22S + 22R), and the sterane C_{29} $\beta\beta/(\beta\beta + \alpha\alpha)$ could all be efficiently utilized to depict organic facies maturity (Welte and Tissot 1984; Bordenave 1993; Peters, Walters, and Moldowan, Peters,

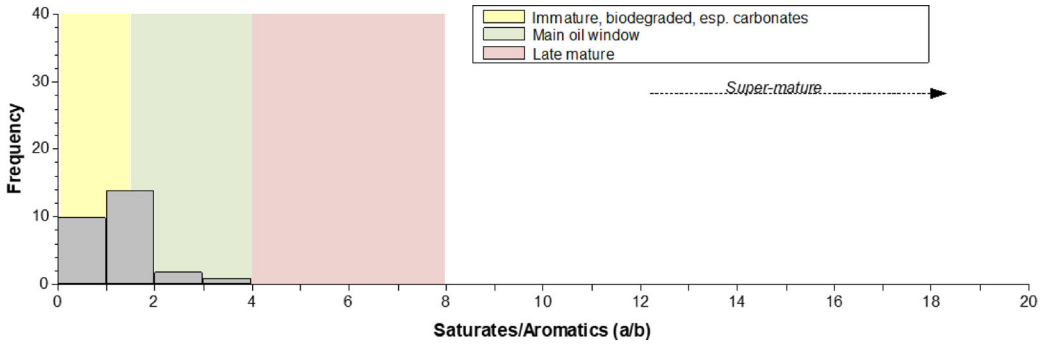

Figure 7E. Generation from the Saturates/Aromatics ratio.

Walters, et al. 2005; Yelwa et al. 2022). The term "paleo-geothermometer" refers to VRo, which is the most widely used technique for determining the optimal paleotemperature and timeframe at any point in geological history (Barker and Elders 1981; Mukhopadhyay 1994) through microscopic examination of kerogens or whole mounts, with a photomultiplier recording the particle's reflectivity. Wells examined are penetrated deep depths of 820–4232 m and have varying thermal maturities, ranked in the oil generation window from premature to the post-mature gas generation stage. In this study, each sampling unit received approximately 30 measurements, and the VR readings avoided reworked vitrinitic materials and inter-maceral effects (Teichmüller, Taylor, and Littke 1998). With concerns about preventing reworked vitrinite, cavings, mud, or hydrocarbon impregnation, and inter-maceral impacts, VRo has been the best measure for recognizing the rank or maturity of sediments (Welte and Tissot 1984; Sweeney and Burnham 1990; Mukhopadhyay 1994; Hunt 1995; Teichmüller, Taylor, and Littke 1998).

In general, immature organic facies has <0.5% Ro, the oil window is 0.5–1.3% R. When Ro is between 1.3 and 2.0%, wet gas is produced; when Ro is greater than 2.0%, dry gas is produced (Welte and Tissot 1984; Sweeney and Burnham 1990; Hakimi, Al-Matary, and Hersi 2018). In essence, < 0.5% Ro immature source rocks; 0.5–0.70% Ro (early oil window generation); 0.70–1.00 (peak oil window generation); 1.00–1.30% Ro (late oil window generation) and >1.3% Ro (post mature gas window generation) as illustrated in Figure 7(A).

Thus, the investigated shales have VRo values between 0.54 and 1.63%, suggesting early oil maturity to post-mature gas generation windows (Figure 7(A)). It shows that 30 of the examined shales are dominantly early and peak oil maturity, with few organofacies in the late oil stage and some samples in the post-mature gas generation window. The variation in optical properties (0.54–1.63 VRo%) is primarily due to mineral structure (Goodarzi et al. 2015), different sub-maceral (Goodarzi 1985), and environments abounding in hydrogen, giving rise to vitrinite suppression (Gentzis and Goodarzi 1994). The thermal variation of biomass in the investigated siliciclastic segments has been directly linked using various positive trends. Specifically, the calibrated VRo (Figure 7(A)), Tables 2 and 4 show T_{max} (Figure 7(B,C)) or even PI details (Figure 7(D)). Consequently, thermal alteration in the studied sediments breaks the kerogen, releasing hydrocarbons. A crucial geochemical criterion to evaluate the probabilistic heat maturity characterizes elevated shale flow rates (Jarvie et al. 2007). This study also explores the association between the depth and VR of the examined shales (Figure 7(A)). It illustrates that changes in reflectance scope, as demonstrated by VR trajectories in the wells studied, affected their thermal maturity (Figure 7(A,C)). The assessment of the samples was consistent and well linked to burial depths (Figure 7(A,B)). The maximum pyrolysis (T_{max}) temperature range is also widely employed as a measure for maturing kerogens (Figure 7(B)). In addition to the VR maturity indicator (Figure 7(A)), T_{max} is often employed to evaluate the maturity of kerogens (Figure 7(B)); their T_{max} rates rise when mature (Bordenave 1993; Espitalié, Deroo, and Marquis 1986; Peters 1986; Tissot, Pelet, and Ungerer 1987; Killops and Killops 2013). The shale samples examined differ from 425 to 476 °C T_{max} values (Figure 7(B); Tables 2 and 4). Eight samples examined exhibit T_{max} values between 435 and 470 °C that vary between early to late maturity (Figures 6(A) and 7(B)). This agrees with the VRo data (VRo 0.68–1.27%). Some samples, such as KFI 1385 and KH1-4232, are over mature, as evidenced by T_{max} (473–476 °C) and high VRo values (1.24–1.37). However, the T_{max} values are very low in 10 samples inspected, which may be ascribed to various impacted variables such as migrating HCs, oil-based muds, low pyrolytic response leading to weakly resolved peaks (Espitalie, Deroo, and Marquis 1985). The low T_{max} values (<430 °C) are compatible with their VRo values ranging between 0.54 and 0.58, with few exceptions like KE1-1480 in the early window. Their burial depths are imprecise insufficient to fulfil all the thermal maturation criteria. In this regard, the state of thermal maturity is evidenced by PI results acquired (Table 2). A ratio of 0.10, for example, indicates immature organic matter, whereas a PI value of 0.10–0.40 indicates mature samples (Hazra et al. 2019; Peters 1986). Its PI info is used in the main stage of oil production for most examined shales is between 0.11 and 0.71, depicting immature *via* mature investigated sediments (Figure 7(D)) as following other maturation results (Figure 7(E)).

5.3. Shale gas-generation potential

Technical advances in producing natural gas from shale deposits at cost-effective rates have unveiled fascinating

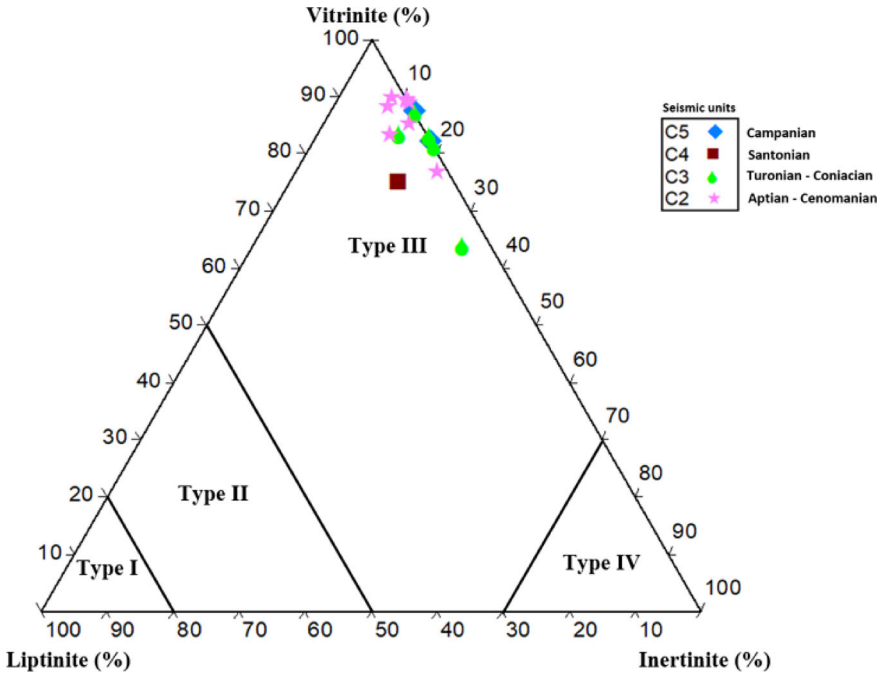

Figure 8A. Triangular diagram illustrating Petroleum generation elucidated using macerals (modified after Hakimi et al. 2020) showing gas-prone preponderance.

frontiers for global crude oil exploration and production. Following the tremendous success of yield in North America, the significance of shale oil and natural gas has piqued international attention. Clearly defining the geology, geochemistry, and geomechanical properties of shale rocks is critical to the success of drilling (e.g., Radwan et al. 2022; Abdelghany et al. 2021), exploration tasks (e.g., Vengosh et al. 2013; Liu et al. 2019; Wenzhi et al. 2020), and achieving optimal yield (e.g., Maxwell 2011; Martinez-Gomez et al. 2017). Even though there are no single, well-defined standard values for different parameters that allow for the measurement of shale gas prospect (Wang and Wang 2016, Sohail, Radwan, and Mahmoud 2022), attempting to compare unproven potentials to physico-chemical parameters measured on known shale gas producers provides a sound basis for screening shale gas representatives. Some key evaluation parameters exist, such as shale layer thickness, TOC, thermal evolution level of organic matter (Ro), and late-stage structural preservation (Zhang et al. 2022). Discrepancies in these parameters result in variable gas content in shale layers, making geological conditions in the Orange Basin complex due to significant variations and extensive gaps. In the Orange Basin, the real hurdle is evaluating the shale with scant information and samples. As a result, companies have yet to begin exploring the Orange Basin's shale gas resources. Orange Basin shale gas development may follow three stages like that of China: conceptual drafting and preparation; regional exploration and industrial practice; and exploratory assessment and industrial growth (Zhang et al. 2022). We evaluate and rank prospective shale gas field in this study to persuade oil companies to consider shale gas expansion. Thus, in this work, an integrated evaluation has been utilised to examine the shale gas potential of different Orange Basin shales and identify significant data gaps that exist that must be resolved in the future to ensure a more favourable evaluation.

The shale gas-generation potential was evaluated based on organic matter quantity, quality, and its maturity with temperature through time (Ardakani et al. 2017; Dow 1977; Peters and Cassa 1994). In this regard, sediment features, kerogen typing, and maturities were deduced by incorporating pyrolysis and microscopic observations to describe its Cretaceous shale sediments, thereby giving information on their potentialities to generate gas within the South African Orange Basin. According to the geochemical results, the analysed Cretaceous samples have good generation potential and can generate significant amounts of HCs (Figures 4 and 7(D,E)).

Aside from organic material amounts, organic facies are critical for forecasting petroleum generation opportunities in the future. Qualitative and quantitative geochemical data show that the samples evaluated had also HI less than 200 mgHC/gTOC; primarily type III kerogens with trace amounts of type IV (Figure 6(A,B)). Accordingly, the discussed Cretaceous shales in the study site are significant source rocks to produce large amounts of gas, as indicated by the TOC and HI cross plot (Figure 6(C)). The high potential for gas-generation resources from these shale sediments is evident by evaluating the maceral composition data (Table 1) and confirmed by the high proportion of vitrinite materials (Figure 8(A,B)).

5.3.1. Source rock interval

The potential Shale-gas successions laterally extend across the 4 K-wells at depths of generally 820–1480m; 1170–2970 m; 1370–1565 m and between 2825 and 4232 m with a thickness of about 660 m; 1800 m; 195 m and 1407 m, respectively, within the basin. These studied shales were

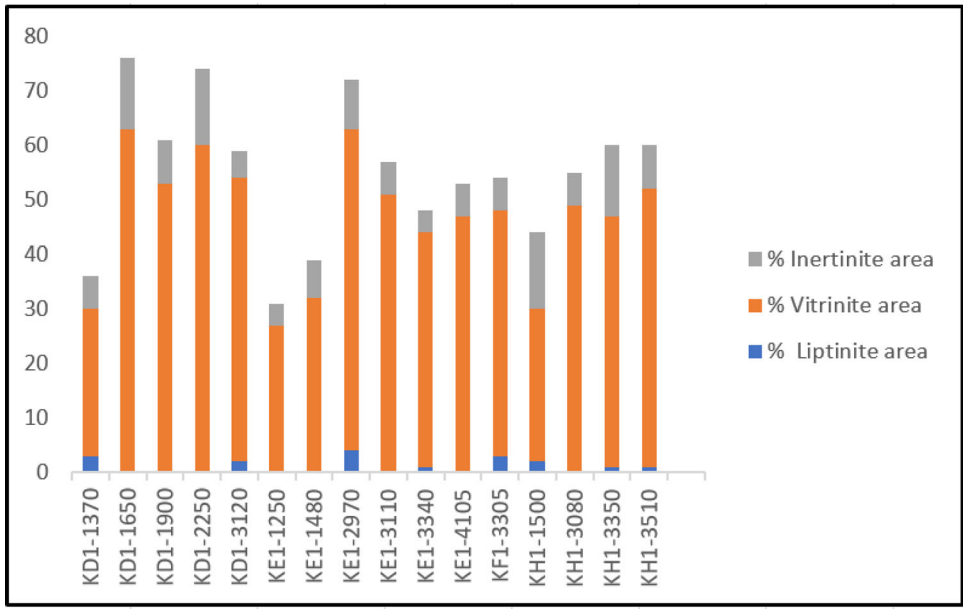

Figure 8B. Average composition of maceral.

categorized from 4 seismic units based on the proven and probable source rock intervals focusing principally on Aptian to Cenomanian sequence (C2) considering its extensive coverage.

5.3.1.1. Campanian source rock interval (C5). These are mostly clay-rich siliceous, non-calcareous mudstone appearing only at KE1 and K-F1 wells between depths 820 and 1480 m. TOC values range from 0.82 to 1.24 wt.% with a mean of 1.05 wt.%. The greatest values (>1 wt.%) occur at KE1-1250. This 660 m sequence is enriched with Mg, BaO, and P_2O_5 (Table 4), averagely making up to 3.44, 0.14, 0.19%, respectively confirming its dolomitic nature and suggesting increased paleo-productivity during deposition as reflected by the occurrence of phosphate intervals and barites. Of 428–473 °C signifying immature *via* late and post-mature gas production and possibly emanate dry gas at 473 °C within lower Campanian KFI 1385 m depth. Low free hydrocarbons (S_1) ranging from 0.08 to 0.49 mg HC/g. Hydrocarbon generated during pyrolysis (S_2) is between 0.47 and 1.28 mg HC/g (averagely 0.80 mg HC/g) with an average generation potential 17.5 bbl oil/ac-ft. This indicates a low potential to generate gas during further burial.

5.3.1.2. Santonian source rocks (C4). This sequence primarily comprises clay-rich carbonaceous mudstone with TOC values from 0.92 to 1.12 wt.% with a mean of 1.00 wt.%. The highest value of 1.12 wt.% occurs at K-FI 1565 m. This 195 m succession contains Mg, BaO, and P_2O_5 (Table 4) averagely of 3.03, 0.08, and 0.19%, recognizing that dolomites have increased paleo-productivity. The peak pyrolysis temperature varies 425–4640 °C, implying immature to late oil window generation. Low S_1 ranged from 0.16 to 0.52 mg HC/g, and S_2 values from 0.61 to 1.41 mg HC/g (average 1.01 mg HC/g). Similarly, the generation potential of these Santonian sediments could be averagely up to 22 bbl oil/ac-ft.

5.3.1.3. Coniacian-Turonian source rocks (C3). It is mostly shale typical organic-rich facies with TOC values between 0.8 and 1.68 wt.% with a mean of 1.16 wt.%. The highest values (>1 wt.%) occur within the KD1-2245-2260, having 1.68 wt.%. Generally, the 1800 m package is also composed of Mg, BaO, and P_2O_5 (Table 4) averagely of 2.53, 0.06, and 0.20%, with more P_2O_5 than other intervals signifying greater paleo-productivity during deposition as reflected by its occurrence. This sequence has rock-eval S_1 between 0.16 and 0.36 mg HC/g averagely 0.23 mg HC/g and S_2 value from 0.90 to 1.26 mg HC/g (averagely 1.08 mg HC/g). S_2/S_3 values indicate that some sections are fairly gas-prone. Also, the generation potential of these sediments is possibly more than 24 bbl higher than all investigated intervals. Its peak pyrolysis temperature varies from 425 to 443 °C, implying immature to early mature levels. This indicates a promising potential to generate oil and gas during other burial conditions.

5.3.1.4. Upper Aptian-Cenomanian source rock (C2). This is the most extensive succession spanning different types of rock units, including upper Albian claystone deposited on the upper slope, Cenomanian organic-rich shales, and some Aptian argillaceous siliceous mudstones. TOC value is between 1.20 and 1.97 wt.%, an average of 1.47 wt.%. Generally, 1407 m package lies within 2825–4232 m also composed of Mg, BaO, and P_2O_5 (Table 4) averagely of 2.09, 0.35, and 0.17%, respectively, which confirms the succession's dolomitic nature, and suggests increased paleo-productivity during deposition as enriched in $Ca(Mg)CO_3$ and phosphorite thereby aiding chemostratigraphy between the Barnet shales, Upper Ecca Southern Karoo sediments and Orange basin shales (Table 5). It composes of rock-eval S_1 from 0.13 to 0.55 mg HC/g, S_2 = 0.8–1.81 mg HC/g. S_2/S_3 values represent fair, gas-prone shale that may generate gas as also affirmed by the highest pyrolysis temperature ranging from 430 to 476 °C, implying immature *via* late mature to post mature stages. This connotes a higher tendency for wet

Table 5. Comparative Study of the Barnett Shale, Upper Ecca and Orange Basin shale gas potentials

	Upper Ecca, Southern Karoo (Chere, 2015)	Barnett, USA. (Bruner and Smosna, 2011)	Orange Basin, South Africa	
			Coniacian- Turonian unit (C3)	Aptian-Cenomanian unit (C2)
TOC	1-2%	2-6%	0.80-1.68%	1.20-1.97%
Kerogen Type	Type II and/or Type III	Type II	Type III	Type III
Mineralogy	>40% quartz	40-50% quartz	56.32-63.31% quartz	57.21-62.19% quartz
Vitrinite reflectance	1-4%	1-2%	0.54-0.86%	0.72-1.63%
Tmax	≥455 °C	≥465 °C	425-443 °C	430-476 °C
Shale porosity	0.5-1.5%	3-6%	6.2%	4-13%
Thickness	1, 300 m	100 m	1,800m	1,407m
Estimated yield	65-400 Tcf	1-40 Tcf	24 bbl oil/ac-ft	30 bbl oil/ac-ft

and dry gas production capacity. In this sequence, there exist KH1-3510 and KH1-4232 having high T_{max} showing its inertness. Furthermore, the generation potential of these sediments is plausibly more than 30 bbl. of oil per ac-ft. greater than that of all explored cycles.

The examined shales show uniform TOC content with depth (about 2 wt.%) with intervals enriched in dolomite within the Campanian succession and phosphorite at the Coniacian and Cenomanian sequences. At the same time, the Cenomanian KH1-3350m contains the most abundant barite of up to 1.10%, allowing chemostratigraphic correlations among different rock units. The hydrocarbon yield during Rock-Eval pyrolysis also vary considerably with depth, with the enormous Aptian-Cenomanian succession having S_1; 0.34 mg HC/g, while S_2; 1.38 mg HC/g on average, shows a limited potency for a gas generation with T_{max} varying from 430 to 476 °C, asserting immature to mature and post mature generation of Type III and III/IV Kerogens. The geochemical mechanisms and shale properties affecting the production, accumulation, and availability of this gas resource throughout Orange Basin are similar to those of the Barnet shale in the Fort Worth Basin. These attributes include organic richness, hydrogen index, the thickness of strata, gas prospects, response to stimulation efforts, and some level of brittleness; as such of great potential for use as a good shale gas resource.

5.3.2. Hydrocarbon volume generated

The generation of petroleum through immature source rocks corresponds directly to the original quantity and the thermal maturation history of generated organic carbon (GOC). Two most likely shale gas successions are at the Coniacian-Turonian and Upper Aptian- Cenomanian with

$$\%\ GOC\ in\ TOC_o = HI_o/1176\ (Jarvie\ 2012)$$

$$HI_o\ of\ 1176 = 85\%\ of\ 1/0.085\ for\ carbon\ in\ hydrocarbons$$

$$TOC_o\ ^*\ \%\ GOC_o = GOC_o\ wt\%$$

$$S_{2o} = GOC_o\ wt.\ \%/0.085$$

$$S_{2o} = HI_o/100^*TOC_o$$

$$S_{2o} = 91/100^*1.31 = 1.19\ mgHC/grock$$

where S_{2o} is the initial hydrocarbon generation tendency in milligram of HC per gram of rock. Therefore, the mean TOC value of the immature Coniacian-Turonian sediments (1.31 wt.%) will generate based on the mean VRo (0.56) of 91 mg/gTOC.

Essentially, S_{2o} is utilized by consideration of thermal maturity and kerogen conversions to determine maximum hydrocarbon yield. Suppose 35°API of oil (0.85 g/cc) as a matrix density of 2.5 g/cc, converted S_{2o} from HC/g rock to barrels of oil equivalent/acre-foot (boe/acre-ft) using a correction factor of 22.82 (Jarvie 2014). The petroleum yield is about 27 boe/ft^3 for the 91HI_o sample at a 50% transformation ratio (TR). Multiplying 27 boe/ft^3 with a source rock thickness of 1800 m gives projected propensity for oil generation in boe/section (Jarvie 2014). Expulsion effects are expected to be validated when estimating the residual oil values or putative hydrocarbon charge for such a combination (Jarvie 2014).

This is one of the most efficient methods in which TOCo, S_{2o}, and HIo may be evaluated in determining immature shales that resemble higher mature sediments. This leads mainly to a range of values of TOC_o and HIo. Typically, the remaining potential of hydrocarbons from Orange basin rocks is evaluated using S_2. According to the analysis, a mean immature siliciclastic sample has an S_{20} of 1.19mgHC/g rock, equating to 27 bb/ac-ft.

The concentration of hydrogen available in the system producing wet and dry gas restricts oil cracking into gas. Oil has an atomic H/C ratio of almost 1.8 H/C relying on the content, whereas methane involves 4.0 hydrogen ions for each carbon. As a result, once it is split into methane, roughly 55% of hydrogen is lacking in oil (Jarvie 2015). However, the losses induced by petroleum expulsion would further decrease the shale system's gas generation potential. Also, S_3, which produces carbon (IV) oxide and carbon monoxide in a small proportion of TOC in terms of mass, is another organic carbon inside kerogens (0.027 × S_3 value). Thus, S_3 computed value is 0.038 and is not linked to oil-generating potential for the examined Orange basin shales. Nevertheless, carbon (IV) oxide has a function in carbon dioxide production, which may lead to carbonate dissociation or juxtaposition (Jarvie 2015).

5.3.3. Expulsion efficiency

The orange basin source rocks have released hydrocarbons into conventional oil and gas reserves. Kudu gas field was explored for more likely prospects in 1974 (Brown 1997). In 1997, Oribi plus Oryz fields produced fewer than 5,000 barrels per day for domestic consumption (Adekola and Akinlua 2013). The AK2 well yields 30 million ft^3 gas with some 600 barrels of condensate at a flow rate of 2200 psi (Berge et al. 2002). AW1 well has two thick, porous

(permeable) discrete reservoir sands but still has low gas saturation water. The AY1 wet well was drilled in the two reservoir sands for 71 million ft^3/d, 1340 bc/d. Amongst wells in the Orange Basin, the AY1 well was tested to contain the highest gas rate in the history of South African fields (Berge et al. 2002). The silica content distribution is critical in determining which wells have the best expulsion ability (Kent 2003). Similarly, the mineralogical composition of shales (Table 4), particularly the calcific content and quartz, influences the formation of fractures (Ding et al. 2012; Jarvie 2011). This same silica concentration in the Campanian KF1-820m is lower than in the Turonian shales, which vary from 51.01 to 63.31% (Table 4), and Turonian KE1-2970 accounts for the vast majority of the SiO_2. Al_2O_3 content is lowest in Campanian KF1-820m, ranging from 12.33 to 17.91% in Cenomanian KF1-3036m. Cao comes in various concentrations, ranging from 1.56 to 11.81%. The silica dominance is based on the fundamental analysis conducted and established by the tests of radiolarian and plankton (Davies 1997). The presence of clays, silica, and calcite reduces the porosity and permeability of sandstones, contributing to the reservoir's poor quality (PASA 2003). The studied shale becomes hard and brittle because of reasonable clastic (silica and certain carbonates) that permits the expulsion of the hydrocarbons. The fragility of the shale is crucial to stimulating the creation of a fracture network that links wellbore with micro-porosity. Although fractures are needed for optimum production in the study area, macro fractures are close to major fault zones, such as AK1; since fractures are loaded with calcareous cement, AK2 is far less productive and perceptive (Berge et al. 2002). Faults could also be used to stimulate energy rather than spalling the calcified shale. Such a response is unlikely to occur in micro-porosity due to poor shale gas wells, notably where faults exist. The prospective shale gas network may be sealed above and, in some locations, under the shale with calcareous or dolomite strings. The fracture thresholds of this limestone are usually more significant than the shale itself, preventing the stimulation of the fracture of the gas-containing shale.

Free oil contents (S_1) are computed on a particular rock as a minimum value due to shortfalls from the shale's recovery, refining, storage, and handling. The gases can be biogenic or thermogenic, but all gases can be indigenous (Figure 5). S_1 oil yields with revived evaporation loss contain movable oil fractions, while pyrolysed oil yields are less movable. GOR is calculated after the production cycle and elevated GORs (>1000 scf/stb) are typically supposed to carry hydrocarbons out of examined samples.

6. Conclusions

In this article, large-scale pyrolysis and visual assessments were used to typify the rocks in the Cretaceous siliciclastic of South Africa's west coast and central Orange Basin. This is essential to identify the outcomes listed below.

1. The analysed shales are good source rocks for petroleum generation because their TOC composition is typically sufficient to generate hydrocarbons.
2. In terms of organic facies (kerogen type), most analysed shales mainly contained Type III and low amounts of Type IV kerogens due to low HI values (40–133 HC/g TOC). This reconfirmed their gas-generation potential.
3. The low proportion of liptinite and inertinite macerals and the dominant NSO components confirmed the hydrogen-poor kerogens and high gas-generation potential.
4. Organic matters in the studied sediments are currently at varying petroleum generation points, ranging from immature to post-mature levels, based on geochemical T_{max} (425–476 °C) and vitrinitic reflectance data of greater than 0.50% VRo and slightly more than 1.60% Ro. Hence, the organic matter intervals in these shales (mainly Type III kerogen) indicate a solid wet and dry gas output tendency. This is because the organic-rich thick shale gas retains part of liquid hydrocarbons to be cracked to gas.
5. The Orange basin shales are organic-rich, type III, gas-prone shales that initially measured around 1.29 wt.% TOC, and HI was somewhat below 100 mg HC/g. Therefore, calculating the earliest PY potential (S_{2o}) holds 1.19 mgHC/g rock and can generate up to 27 bbl oil/ac-ft.
6. All the geological and geochemical properties of the Orange Basin shales studied are promising regarding shale gas potential. However, in detail, geo-mechanical data is required before any further conclusions about the productive capacity of these gas shales can be drawn.
7. This study can be used for new gas exploration and production in the Orange basin in known low-lying areas where these sediments reach high burial temperatures in the window for gas generation.

Acknowledgements

The authors gratefully acknowledge the University of Malaya research grant (IF064-2019) and the study support provided by Usmanu Danfodiyo University Sokoto *via* TeTFUND intervention. Furthermore, special appreciation goes to Mr Zamri, Aliff, and Madam Zaleha for their analytical assistance. Finally, we would like to express our gratitude to Integrated Geochemical Interpretation (IGI) Ltd for providing an academic license for the p: IGI geochemical software.

Disclosure statement

The authors declare that they have no known competing financial interests or personal relationships that could appear to have influenced the work described in this article.

Funding

This work was supported by Institut Pengurusan dan Pemantauan Penyelidikan; Universiti Malaya; TETFund National Research Fund.

ORCID

Nura Abdulmumini Yelwa http://orcid.org/0000-0002-7454-2326

References

Abdelghany, W. K., A. E. Radwan, M. A. Elkhawaga, D. A. Wood, S. Sen, and A. A. Kassem. 2021. Geomechanical Modeling Using the Depth-of-Damage Approach to Achieve Successful Underbalanced Drilling in the Gulf of Suez Rift Basin. *Journal of Petroleum Science and Engineering* 202: 108311. doi:10.1016/j.petrol.2020.108311.

Adegoke, K. A. 2015. *Source Rock Characterisation and 1D Basin Modelling of the Upper Cretaceous Sediments*. Kuala Lumpur, Malaysia: Chad (Bornu) Basin, Northeastern Nigeria Jabatan Geologi, Fakulti Sains, Universiti Malaya.

Adekola, S. A., and A. Akinlua. 2012. Source Rock Characterization within the Stratigraphic Settings of the Orange Basin. *South Africa. Petroleum Science and Technology* 30 (6): 545–558. doi:10.1080/10916466.2010.481652.

Adekola, S. A., A. Akinlua, and K. Mangelsdorf. 2012. Organic Geochemical Evaluation of Cretaceous Shale Samples from the Orange Basin. *South Africa Applied Geochemistry* 27 (8): 1633–1642. doi:10.1016/j.apgeochem.2012.03.012.

Adekola, S. A., and A. Akinlua. 2013. Petrography and Stable Isotope Geochemistry of Cretaceous Sandstones, Orange Basin, South Africa. *Journal of Petroleum Exploration and Production Technology* 3 (2): 69–83. doi:10.1007/s13202-013-0050-5.

Ardakani, O. H., H. Sanei, A. Ghanizadeh, M. McMechan, F. Ferri, and C. R. Clarkson. 2017. Hydrocarbon Potential and Reservoir Characteristics of Lower Cretaceous Garbutt Formation, Liard Basin Canada. *Fuel* 209: 274–289. doi:10.1016/j.fuel.2017.07.106.

Africa, A. S. 2016. South Africa's technical readiness to support the shale gas industry. https://research.assaf.org.za/handle/20.500.11911/14

Akinlua, A., A. Sigedle, T. Buthelezi, and O. A. Fadipe. 2015. Trace Element Geochemistry of Crude Oils and Condensates from South African Basins. *Marine and Petroleum Geology* 59: 286–293. doi:10.1016/j.marpetgeo.2014.07.023.

Atkinson, D. 2018. Fracking in a Fractured Environment: Shale Gas Mining and Institutional Dynamics in South Africa's Young Democracy. *Extractive Industries and Society-an International Journal*, 5 (4): 441–452. doi:10.1016/j.exis.2018.09.013.

Barker, C. E., and W. A. Elders. 1981. Vitrinite Reflectance Geothermometry and Apparent Heating Durationin the Cerro Prieto Geothermal-Field. *Geothermics* 10 (3–4): 207–223. doi:10.1016/0375-6505(81)90005-5.

Berge, T. B., F. Aminzadeh, P. de Groot, and T. Oldenziel. 2002. Seismic Inversion Successfully Predicts Reservoir, Porosity, and Gas Content in Ibhubesi Field, Orange Basin, South Africa. *The Leading Edge* 21 (4): 338–348. doi:10.1190/1.1471595.

Bissada, K. K. 1982. Geochemical Constraints on Petroleum Generation and Migration—a Review. *Proceedings ASCOPE* 81: 69–87. doi:10.1177/0144598793011003-405.

Bordenave, M. 1993. Screening Techniques for Source Rock Evaluation. *Applied Petroleum Geochemistry* 217–278. https://cir.nii.ac.jp/crid/1570572699993218048.

Bilgen, S, and I. Sarikaya. 2016. New Horizon in Energy: Shale Gas. *Journal of Natural Gas Science and Engineering* 35: 637–645. doi:10.1016/j.jngse.2016.09.014.

Broad, D. S., E. H. A. Jungslager, I. R. McLachlan, J. Roux and D. van der Spuy. 2012. South Africa's offshore Mesozoic basins. *Geological Society of South Africa, Johannesburg/Council for Geoscience, Pretoria* : 553–571. doi:10.1016/b978-0-444-56357-6.00014-7.

Brown, L. F. 1997. AAPG Studies in Geology No 41 - Sequence Stratigraphy in Offshore South African Divergent Basins; an Atlas on Exploration for Cretaceous Lowstand Traps by Soekor (Pty) Ltd - Reply. *Marine and Petroleum Geology* 14 (4): 469–470. doi:10.1016/s0264-8172(97)00020-2.

Bruner, K. R., and R. A. Smosna. 2011. *A Comparative Study of the Mississippian Barnett Shale*. Pittsburgh, PA: Fort Worth Basin, and Devonian Marcellus Shale, Appalachian Basin, US Department of Energy, National Energy Technology Laboratory, DOE/NETL-2011/1478.

Caineng, Z., D. Dong, S. Wang, J. Li, X. Li, Y. Wang, D. Li, and K. Cheng. 2010. Geological Characteristics and Resource Potential of Shale Gas in China. *Petroleum Exploration and Development* 37(6): 641–653. doi:10.1016/S1876-3804(11)60001-3.

Caineng Z., D. Dong, Y. Wang, X. Li, J. Huang, S. F. Wang, Q. Z. Guan, C. C. Zhang, H. Y. Wang, H. L. Liu, W. H. Bai, F. Liang, W. Lin, Q. Zhao, D. X. Liu, Z. Yang, P. P. Liang, S. S. Sun, and Z. Qiu. 2015. Shale Gas in China: Characteristics, Challenges and Prospects (I). *Petroleum Exploration and Development* 42 (6): 753–767. doi:10.1016/s1876-3804(15)30072-0.

Chere, N. 2015. *Sedimentological and Geochemical Investigations on Borehole Cores of the Lower Ecca Group Black Shales, for Their Gas Potential: Karoo Basin, South Africa*. Port Elizabeth, South Africa: Nelson Mandela Metropolitan University

Chere, N., B. Linol, M. De Wit, and H. M. Schulz. 2017. 2017. Lateral and Temporal Variations of Black Shales across the Southern Karoo Basin-Implications for Shale Gas Exploration. *South African Journal of Geology* 120 (4): 541–564.

Cooles, G. P., A. S. Mackenzie, and T. M. Quigley. 1986. Calculation of Petroleum Masses Generated and Expelled from Source Rocks. *Organic Geochemistry* 10 (1–3): 235–245. doi:10.1016/0146-6380(86)90026-4.

Curtis, J. B. 2002. Fractured Shale-Gas Systems. *Aapg Bulletin* 86 (11): 1921–1938. doi:10.1306/61eeddbe-173e-11d7-8645000102c1865d.

Davies, C. P. 1997. Unusual Biomarker Maturation Ratio Changes through the Oil Window, a Consequence of Varied Thermal History. *Organic Geochemistry* 27 (7–8): 537–560. doi:10.1016/s0146-6380(97)00059-4.

Ding, W., C. Li, C. Li, C. Xu, K. Jiu, W. Zeng, and L. Wu. 2012. Fracture Development in Shale and Its Relationship to Gas Accumulation. *Geoscience Frontiers* 3 (1): 97–105. doi:10.1016/j.gsf.2011.10.001.

Dow, W. G. 1977. Kerogen Studies and Geological Interpretations. *Journal of Geochemical Exploration* 7: 79–99. doi:10.1016/0375-6742(77)90078-4.

EIA, U. 2014. Annual Energy Outlook 2014 with projections to 2040, April 2014, A-25, 269. DOE/EIA-0383. https://www.eia.gov/analysis/projection-data.php.

EIA, U. 2015. World Shale Resource Assessments. *Government. EIA/Analysis/Studies/World Shale Gas*, September, 24. https://www.ieee.es/Galerias/fichero/OtrasPublicaciones/Internacional/2015.

EIA, U. 2013. Technically Recoverable Shale Oil & Gas Resources: An Assessment of 137 Shale Formations in 41 Countries outside the US. June. http://www.eia.gov/analysis/studies/worldshalegas.

Espitalie, J., G. Deroo, and F. Marquis. 1985. La Pyrolyse Rock-Eval et Ses Applications. *Revue de L'Institut Français du Pétrole* 40 (5): 563–579. doi:10.2516/ogst:1985045.

Espitalié, J., G. Deroo, and F. Marquis. 1986. La Pyrolyse Rock-Eval et Ses Applications. Troisième Partie. *Revue de L'Institut Français du Pétrole* 41 (1): 73–89. doi:10.2516/ogst:1986003.

Fatti, J. L., G. C. Smith, P. J. Vail, P. J. Strauss, and P. R. Levitt. 1994. Detection of Gas in Sandstone Reservoirs Using AVO Analysis: A 3-D Seismic Case History Using the Geostack Technique. *Geophysics* 59 (9): 1362–1376. doi:10.1190/1.1443695.

Gentzis, T, and F. Goodarzi. 1994. *Reflectance Suppression in Some Cretaceous Coals from Alberta, Canada*. Washington, DC: ACS Publications.

Gerrard, I, and G. C. Smith. 1982. Post-Paleozoic Succession and Structure of the Southwestern African Continental Margin: Rifted Margins: Field Investigations of Margin Structure and Stratigraphy. In *Studies in Continental Margin Geology*, Vol. M34, 49–74. AAPG Memoir. https://archives.datapages.com/data/specpubs/history2/data/a110/a110/0001/0000/0049.htm.

Goodarzi, F. 1985. Organic Petrology of Hat Creek Coal Deposit No. 1, British Columbia. *International Journal of Coal Geology* 5 (4): 377–396. doi:10.1016/0166-5162(85)90003-5.

Goodarzi, F., O. H. Ardakani, P. K. Pedersen, and H. Sanei. 2015. Canadian Arctic Oil Shale Resources: A Re-Assessment of Potential Ordovician to Carboniferous Oil Shale Deposits. In *OTC Arctic Technology Conference*. OnePetro. doi:10.4043/25576-MS.

Hackley, P. C., and B. J. Cardott. 2016. Application of Organic Petrography in North American Shale Petroleum Systems: A

Review. *International Journal of Coal Geology* 163: 8–51. doi:10.1016/j.coal.2016.06.010.

Hakimi, M. H., A. Ahmed, A. Y. Kahal, O. S. Hersi, H. J. Al Faifi, and S. Qaysi. 2020a. Organic Geochemistry and Basin Modeling of Late Cretaceous Harshiyat Formation in the Onshore and Offshore Basins in Yemen: Implications for Effective Source Rock Potential and Hydrocarbon Generation. *Marine and Petroleum Geology* 122: 104701. doi:10.1016/j.marpetgeo.2020.104701.

Hakimi, M. H., W. H. Abdullah, A. A. Lashin, E. H. Ibrahim, and Y. M. Makeen. 2020b. Hydrocarbon Generation Potential of the Organic-Rich Naifa Formation, Say'un-Masila Rift Basin, Yemen: Insights from Geochemical and Palynofacies Analyses. *Natural Resources Research* 29 (4): 2687–2715. doi:10.1007/s11053-019-09595-1.

Hakimi, M. H., A. M. Al-Matary, O. El-Mahdy, B. A. Hatem, A. Y. Kahal, and A. Lashin. 2020c. Organic Geochemistry Characterization of Late Jurassic Bituminous Shales and Their Organofacies and Oil Generation Potential in the Shabwah Depression, Southeast Sabatayn, Yemen. *Journal of Petroleum Science and Engineering* 188Article: 106951. doi:10.1016/j.petrol.2020.106951.

Hakimi, M. H., A. M. Al-Matary, and O. S. Hersi. 2018. Late Jurassic Bituminous Shales from Marib Oilfields in the Sabatayn Basin (NW Yemen): Geochemical and Petrological Analyses Reveal Oil-Shale Resource. *Fuel* 232: 530–542. doi:10.1016/j.fuel.2018.05.138.

Hartwig, A., Z. Anka, and R. di Primio. 2012. Evidence of a Widespread Paleo-Pockmarked Field in the Orange Basin: An Indication of an Early Eocene Massive Fluid Escape Event Offshore South Africa. *Marine Geology* 332–334: 222–234. doi:10.1016/j.margeo.2012.07.012.

Hazra, B., D. A. Wood, D. Mani, P. K. Singh, and A. K. Singh. 2019. *Evaluation of Shale Source Rocks and Reservoirs*. Berlin, Germany: Springer. doi: 10.1007/978-3-030-13042-8.

Hirsch, K. K., M. Scheck-Wenderoth, J. D. van Wees, G. Kuhlmann, and D. A. Paton. 2010. Tectonic Subsidence History and Thermal Evolution of the Orange Basin. *Marine and Petroleum Geology* 27 (3): 565–584. doi:10.1016/j.marpetgeo.2009.06.009.

Hunt, J. M. 1995. *Petroleum Geochemistry and Geology*. 2nd ed. xx–743. New York, NY: W. H. Freeman. ISBN 071624413

Jarvie, D. M. 2011. Shale Resource Systems for Oil and Gas: Part I—Shale Gas Resource Systems. Part II—Shale Oil Resource Systems. *Shale Reservoirs Giant Resources for the 21st Century: AAPG Memoir* 97: 1–31. doi:10.1306/13321447M973489.

Jarvie, D. M., and L. L. Lundell. 1991. Hydrocarbon generation modeling of naturally and artificially matured Barnett Shale, Fort Worth Basin, Texas: Southwest Regional Geochemistry Meeting, September 8 – 9, 1991, The Woodlands, Texas, 1991, http://www.humble-inc.com/Jarvie_Lundell_1991.pdf.

Jarvie, D. M. 2014. Components and Processes Affecting Producibility and Commerciality of Shale Resource Systems. *Geologica Acta* 12 (4): 307–325. doi:10.1344/GeologicaActa2014.12.4.3.

Jarvie, D. M. 2015. Geochemical Assessment of Unconventional Shale Gas Resource Systems. In ed. R. Rezaee, *Fundamentals of Gas Shale Reservoirs*, Chapter 4, Vol. 3, 47–69. John Wiley & Sons. doi:10.1002/9781119039228.ch3.

Jarvie, D. 2012. Shale Resource Systems for Oil and Gas: part I—Shale Gas Resource Systems. Part II—Shale Oil Resource Systems. Shale Reservoirs-Giant Resources for the 21st Century. *AAPG Memoir* 97: 69–87. doi:10.1306/13321446M973489.

Jarvie, D. M., R. J. Hill, T. E. Ruble, and R. M. Pollastro. 2007. Unconventional Shale-Gas Systems: The Mississippian Barnett Shale of North-Central Texas as One Model for Thermogenic Shale-Gas Assessment. *AAPG Bulletin* 91 (4): 475–499. doi:10.1306/12190606068.

Jarvie, D. M., R. J. Hill, R. M. Pollastro, D. A. Wavrek, K. A. Bowker, B. L. Claxton, and M. H. Tobey. 2003. Evaluation of Unconventional Natural Gas Prospects: The Barnett Shale Fractured Shale Gas Model (Abs.). 21st International meeting on organic geochemistry, 3–4; Krakow, Poland: Book of Abstracts, Part II, September 8–12, 2003.

Jones, R. W. 1984. Comparison of Carbonate and Shale Source Rocks. *Aapg Bulletin-American Association of Petroleum Geologists* 68 (4): 160–183.

Jungslager, E. H. 1999. Petroleum Habitats of the Atlantic Margin of South Africa. *Geological Society, London, Special Publications* 153 (1): 153–168. doi:10.1144/GSL.SP.1999.153.01.10.

Katz, B., and F. Lin. 2014. Lacustrine Basin Unconventional Resource Plays: Key Differences. *Marine and Petroleum Geology* 56: 255–265. doi:10.1016/j.marpetgeo.2014.02.013.

Kent, B. 2003. Recent Development of the Barnett Shale Play, Forth Worth Basin. *West Texas Geological Society Bulletin* 42 (6): 4–11. http://www.wtgs.org/.

Killops, V. J., and S. D. Killops. 2013. *Introduction to Organic Geochemistry*. Hoboken, NJ: John Wiley & Sons.

Kuhlmann, G., S. Adams, C. Campher, D. van der Spuy, R. di Primio, and B. Horsfield. 2010. Passive Margin Evolution and Its Controls on Natural Gas Leakage in the Southern Orange Basin, Blocks 3/4, Offshore South Africa. *Marine and Petroleum Geology* 27 (4): 973–992. doi:10.1016/j.marpetgeo.2010.01.010.

Largeau, C, and J. De Leeuw. 1995. *Sedimentary Organic Matter: Organic Facies and Palynofacies: By RV TYSON*, 615. Chapman and Hall, London: doi: Pergamon.ISBN 0-412-36350-X.£115.00.

Li, Y. X., Z. M. Hu, X. G. Liu, S. S. Gao, X. G. Duan, J. Chang, and J. F. Wu. 2018. Insights into Interactions and Microscopic Behavior of Shale Gas in Organic - Rich Nano - Slits by Molecular Simulation. *Journal of Natural Gas Science and Engineering* 59: 309–325. doi:10.1016/j.jngse.2018.09.011.

Li, Y. J., Y. Y. Feng, H. Liu, L. H. Zhang, and S. X. Zhao. 2013. Geological Characteristics and Resource Potential of Lacustrine Shale Gas in the Sichuan Basin, SW China. *Petroleum Exploration and Development* 40 (4): 454–460. doi:10.1016/s1876-3804(13)60057-9.

Liu, J., Z. L. He, X. W. Liu, Z. Z. Huo, and P. Guo. 2019. Using Frequency-Dependent AVO Inversion to Predict the. "Sweet Spots." "Of Shale Gas Reservoirs." *Marine and Petroleum Geology* 102: 283–291. doi:10.1016/j.marpetgeo.2018.12.039.

Magoon, L. B., and W. G. Dow. 1994. The Petroleum System: chapter 1: Part I. Introduction. In *The Petroleum System-From Source to Trap*, 3–24. https://archives.datapages.com/data/specpubs/methodo2/data/a077/a077/0001/0000/0003.htm.

Martinez-Gomez, J., F. Napoles-Rivera, J. M. Ponce-Ortega, and M. M. El-Halwagi. 2017. Optimization of the Production of Syngas from Shale Gas with Economic and Safety Considerations. *Applied Thermal Engineering* 110: 678–685. doi:10.1016/j.applthermaleng.2016.08.201.

Maxwell, S. 2011. Microseismic Hydraulic Fracture Imaging: The Path toward Optimizing Shale Gas Production. *The Leading Edge* 30 (3): 340–346. doi:10.1190/1.3567266.

McMillan, I. K., G. I. Brink, D. S. Broad, and J. J. Maier. 1997. Late Mesozoic Sedimentary Basins off the South Coast of South Africa. *Sedimentary Basins of the World*, Vol. 3, 319–376. Amsterdam, Netherlands: Elsevier. doi:10.1016/S1874-5997(97)80016-0.

Mukhopadhyay, P. K. 1994. Vitrinite Reflectance as Maturity Parameter-Petrographic and Molecular Characterization and Its Applications to Basin Modelling. In eds. P. K. Mukhopadhyay and W. G. Dow, *Vitrinite Reflectance as a Maturity Parameter: Applications and Limitations*, Vol. 570, 1–24. ACS Symposium Series. ISBN 0-8412-2994-5. WOS: A1994BD02F00001. Washington, DC: American Chemical Society,

Mukhopadhyay, P. K., J. A. Wade, and M. A. Kruge. 1995. Organic Facies and Maturation of Jurassic/Cretaceous Rocks, and Possible Oil-Source Rock Correlation Based on Pyrolysis of Asphaltenes, Scotian Basin. *Canada. Organic Geochemistry* 22 (1): 85–104. doi:10.1016/0146-6380(95)90010-1.

Mustafa, A., Z. Tariq, M. Mahmoud, A. E. Radwan, A. Abdulraheem, and M. O. Abouelresh. 2022. Data-Driven Machine Learning Approach to Predict Mineralogy of Organic-Rich Shales: An Example from Qusaiba Shale, Rub' al Khali Basin, Saudi Arabia. *Marine and Petroleum Geology* 137: Article 105495. doi:10.1016/j.marpetgeo.2021.105495.

Mustapha, K. A. 2016. *Petroleum Source Rock Characterization and Petroleum System Analysis of the Neogene Sedimentary Sequences in the Ne Sabah Basin*. Kuala Lumpur, Malaysia: Malaysia Department of Geology, Faculty Science, University Malaya].

Mustapha, K. A, and W. H. Abdullah. 2013. Petroleum Source Rock Evaluation of the Sebahat and Ganduman Formations, Dent Peninsula, Eastern Sabah, Malaysia. *Journal of Asian Earth Sciences* 76: 346–355. doi:10.1016/j.jseaes.2012.12.003.

Osli, L. N., M. R. Shalaby, and M. Islam. 2018. Characterization of Source Rocks and Depositional Environment, and Hydrocarbon Generation Modelling of the Cretaceous Hoiho Formation, Great South Basin, Newzealand. *Petroleum & Coal* 60 (2): 255–275. https://www.vurup.sk/petroleum/2018/volume-60/#volume-60-2018-issue-2.

Paton, D. A., R. Di Primio, G. Kuhlmann, D. Van Der Spuy, and B. Horsfield. 2007. Insights into the Petroleum System Evolution of the Southern Orange Basin, South Africa. *South African Journal of Geology* 110 (2–3): 261–274. doi:10.2113/gssajg.110.2-3.261.

Peters, K. E. 1986. Guidelines for Evaluating Petroleum Source Rock Using Programmed Pyrolysis. *American Association of Petroleum Geologists Bulletin* 70 (3): 318–329. doi:10.1306/94885688-1704-11d7-8645000102c1865d.

Peters, K. E., and J. M. Moldowan. 1993. The biomarker guide: interpreting molecular fossils in petroleum and ancient sediments. https://www.osti.gov/biblio/6066248

Peters, K. E., and M. R. Cassa. 1994. Applied Source Rock Geochemistry. *The Petroleum System - from Source to Trap*, 93–120. Tulsa, OK: AAPG Memoir.

Peters, K. E. Peters, C. C. Walters, and J. M. Moldowan. 2005. *The Biomarker Guide*, Vol. 1. Cambridge: Cambridge University Press.

Peters, K. E., C. Walters, and M. Moldowan. 2005. *The Biomarker Guide: Biomarkers and Isotopes in Petroleum Exploration and Earth History*. Cambridge, NY: Cambridge University Press.

Petroleum Agency of South Africa, P. 2003. *Petroleum Exploration Information and Opportunities*. Brochure Cape Town, South Africa: Petroleum Agency South Africa.

Radwan, A. E., D. A. Wood, M. Mahmoud, and Z. Tariq. 2022. Gas Adsorption and Reserve Estimation for Conventional and Unconventional Gas Resources. *Sustainable Geoscience for Natural Gas Subsurface Systems*, 345–382. Amsterdam, Netherlands: Elsevier.

Sandvik, E. I., W. A. Young, and D. J. Curry. 1992. Expulsion from Hydrocarbon Sources: The Role of Organic Absorption. *Organic Geochemistry* 19 (1–3): 77–87. doi:10.1016/0146-6380(92)90028-v.

Sawada, K. 2006. Organic Facies and Geochemical Aspects in Neogene Neritic Sediments of the Takafu Syncline Area of Central Japan: Paleoenvironmental and Sedimentological Reconstructions. *Island Arc* 15 (4): 517–536. doi:10.1111/j.1440-1738.2006.00546.x.

Schmoker, J. W. 1995. Method for Assessing Continuous-Type (Unconventional) Hydrocarbon Accumulations. In Eds. D. L. Gautier, G. L. Dolton, K. I. Takahashi and K.L. Varnes, National assessment of United States Oil and Gas Resources—Results, Methodology, and Supporting Data: U.S. Geological Survey Digital Data Series, 30. CD-ROM.K.L.K.L.

Scholes, B., P. Lochner, G. Schreiner, Luanita Snyman-An der Walt, and M. De Jager. 2016. Shale Gas Development in the Central Karoo: A Scientific Assessment of the Opportunities and Risks. *Clean Air Journal* 26 (2): 6.

Shalaby, M. R., M. H. Hakimi, and W. H. Abdullah. 2011. Geochemical Characteristics and Hydrocarbon Generation Modeling of the Jurassic Source Rocks in the Shoushan Basin, North Western Desert, Egypt. *Marine and Petroleum Geology* 28 (9): 1611–1624. doi:10.1016/j.marpetgeo.2011.07.003.

Shalaby, M. R., M. H. Hakimi, and W. H. Abdullah. 2012. Organic Geochemical Characteristics and Interpreted Depositional Environment of the Khatatba Formation, Northern Western Desert. *AAPG Bulletin* 96 (11): 2019–2036. doi:10.1306/04181211178.

Shen, W., X. Li, Y. Xu, Y. Sun, and W. Huang. 2017. Gas Flow Behavior of Nanoscale Pores in Shale Gas Reservoirs. *Energies* 10 (6): 751. doi:10.3390/en10060751.

Shen, W., L. Zheng, C. M. Oldenburg, A. Cihan, J. Wan, and T. K. Tokunaga. 2018. Methane Diffusion and Adsorption in Shale Rocks: A Numerical Study Using the Dusty Gas Model in TOUGH2/EOS7C-ECBM. *Transport in Porous Media* 123 (3): 521–531. doi:10.1007/s11242-017-0985-y.

Sohail, G. M., A. E. Radwan, and M. Mahmoud. 2022. A Review of Pakistani Shales for Shale Gas Exploration and Comparison to North American Shale Plays. *Energy Reports* 8: 6423–6442. doi:10.1016/j.egyr.2022.04.074.

Stainforth, J. G., and J. E. A. Reinders. 1990. Primary Migration of Hydrocarbons by Diffusion through Organic Matter Networks, and Its Effect on Oil and Gas Generation. *Organic Geochemistry* 16 (1–3): 61–74. doi:10.1016/0146-6380(90)90026-v.

Suarez-Ruiz, I., D. Flores, J. G. Mendonca, and P. C. Hackley. 2012. Review and Update of the Applications of Organic Petrology: Part 1, Geological Applications. *International Journal of Coal Geology* 99: 54–112. doi:10.1016/j.coal.2012.02.004.

Sweeney, J. J., and A. K. Burnham. 1990. Evaluation of a Simple - Model of Vitrinite Reflectance Based on Chemical - Kinetics. *Aapg Bulletin-American Association of Petroleum Geologists* 74 (10): 1559–1570. doi:10.1306/0C9B251F-1710-11D7-8645000102C1865D.

Taylor, G. H., M. Teichmuller, A. Davis, C. F. K. Diessel, R. Littke, and P. Robert. 1998. Organic Petrology. A new handbook incorporating some revised parts of Stach's Textbook of Coal Petrology. Berlin, Stutgart: Gebruder Borntraeger. https://www.schweizerbart.de/publications/detail/isbn/9783443010362/Taylor_et_al_Organic_Petrology.

Taylor, K. G, and J. H. S. Macquaker. 2014. Diagenetic Alterations in a Silt- and Clay-Rich Mudstone Succession: An Example from the Upper Cretaceous Mancos Shale of Utah, USA. *Clay Minerals* 49 (2): 213–227. doi:10.1180/claymin.2014.049.2.05.

Teichmüller, M., G. H. Taylor, and R. Littke. 1998. The Nature of Organic Matter-Macerals and Associated Minerals. *Organic Petrology*, 175–274. Stuttgart, Germany.

Thomas, M. M., and J. A. Clouse. 1990. Primary Migration by Diffusion through Kerogen: I. Model Experiments with Organic-Coated Rocks. *Geochimica et Cosmochimica Acta* 54 (10): 2775–2779. doi:10.1016/0016-7037(90)90011-9.

Tissot, B. P., R. Pelet, and P. H. Ungerer. 1987. Thermal History of Sedimentary Basins, Maturation Indices, and Kinetics of Oil and Gas Generation. *AAPG Bulletin* 71 (12): 1445–1466. doi:10.1306/703C80E7-1707-11D7-8645000102C1865D.

Van der Spuy, D. 2003. Aptian Source Rocks in Some South African Cretaceous Basins. *Geological Society, London, Special Publications* 207 (1): 185–202. doi:10.1144/GSL.SP.2003.207.10.

Van der Spuy, D., N. A. Jikelo, T. Ziegler, and M. Bowyer. 2003. Deepwater 2D Data Reveal Orange Basin Objectives off Western South Africa. *Oil & Gas Journal* 101 (14): 44–44. https://elibrary.ru/item.asp?id=6280076.

Van Huyssteen, E., C. Green, P. Paige-Green, M. Oranje, S. Berrisford, and D. McKelly. 2016. Impacts on Integrated Spatial and Infrastructure Planning. In eds. R. Scholes, P. Lochner, G. Schreiner, L. Snyman-Van der Walt, and M. de Jager, *Shale Gas Development in the Central Karoo: A Scientific Assessment of the Opportunities and Risks* 18–68. http://researchspace.csir.co.za/dspace/handle/10204/9074.

Vengosh, A., N. Warner, R. Jackson, and T. Darrah. 2013. The effects of shale gas exploration and hydraulic fracturing on the quality of water resources in the United States. Proceedings of the fourteenth international symposium on water-rock interaction, wri 14. 14th International Symposium on Water-Rock Interaction (WRI), Avignon, France. *Procedia Earth and Planetary Science* 7 (2013): 863–866. doi:10.1016/j.proeps.2013.03.213.

Visser, D. J. L., G. Brandl, L. P. Chevallier, D. I. Cole, C. H. de Beer, P. G. Grease, F. J. Hartzer, R. S. Hill, N. Keyser, F. G. le Roux, J. E. J. Martini, H. F. G. Moen, L. W. Schurrmann, J. N. Theron, R. J. Thomas, C. J. Van Vuuren. 1998. The Geotectonic Evolution of South Africa and Offshore Areas. Council for Geoscience, Geological Survey of South Africa. Apparent First Edition, 319 p. https://biblio.co.nz/book/geotectonic-evolution-south-africa-offshore-areas/d/205662913.

Wang, Q., and L. Wang. 2016. Comparative Study and Analysis of the Development of Shale Gas between China and the USA. *International Journal of Geosciences* 07 (02): 200–209. doi:10.4236/ijg.2016.72016.

Wang, H., X. Q. Wang, X. Jin, and D. P. Cao. 2016. Molecular Dynamics Simulation of Diffusion of Shale Oils in Montmorillonite. *The Journal of Physical Chemistry C* 120 (16): 8986–8991. doi:10.1021/acs.jpcc.6b01660.

Welte, D., and P. Tissot. 1984. Petroleum Formation and Occurrence. *A New Approach to Oil and Gas Exploration.* Berlin, Germany: Springer. doi:10.1007/978-3-642-96446-6.

Wenzhi, Z., J. Ailin, W. Yunsheng, W. Junlei, and Z. Hanqing. 2020. Progress in Shale Gas Exploration in China and Prospects for Future Development. *China Petroleum Exploration* 25 (1): 31. http://www.cped.cn/EN/Y2020/V25/I1/31.

Wood, G. 1996. Palynological Techniques-Processing and Microscopy. In *Palynology: Principles and Application. American Association of Stratigraphic Palynologists Foundation*, eds. J. Jasonius, and D. C. McGregor, Vol. 1, 29–50. American Association of Stratigraphic Palynologists Foundation. https://cir.nii.ac.jp/crid/1572543024138151168.

Xingang, Z., K. Jiaoli, and L. Bei. 2013. Focus on the Development of Shale Gas in China—Based on SWOT Analysis. *Renewable and Sustainable Energy Reviews* 21: 603–613. doi:10.1016/j.rser.2012.12.044.

Yelwa, N. A., K. A. Mustapha, M. Opuwari, and A. A. Aziz. 2022. Biomarkers, Stable Carbon Isotope, and Trace Element Distribution of Source Rocks in the Orange Basin, South Africa: Implications for Paleoenvironmental Reconstruction, Provenance, and Tectonic Setting. *Journal of Petroleum Exploration and Production Technology* 12: 307–339. doi:10.1007/s13202-021-01317-9.

Zhang, J., M. Shi, D. Wang, Z. Tong, X. Hou, J. Niu, X. Li, Z. Li, P. Zhang, and Y. Huang. 2022. Fields and Directions for Shale Gas Exploration in China. *Natural Gas Industry B* 9 (1): 20–32.

Zhang, H., X. Zeng, Z. Zhao, Z. Zhai, and D. Cao. 2017. Adsorption and Selectivity of CH_4/CO_2 in Functional Group Rich Organic Shales. *Journal of Natural Gas Science and Engineering* 39: 82–89. doi:10.1016/j.jngse.2017.01.024.